LBL-13697
Preprint c.2

Lawrence Berkeley Laboratory

UNIVERSITY OF CALIFORNIA

Materials & Molecular Research Division

RECEIVED
LAWRENCE
BERKELEY LABORATORY

NOV 16 1982

LIBRARY AND
DOCUMENTS SECTION

Submitted to Physical Review A

ELECTRON SPECTROSCOPY STUDY OF INNER-SHELL PHOTOEXCITATION AND IONIZATION OF Xe

S. Southworth, U. Becker, C.M. Truesdale, P.H. Kobrin, D.W. Lindle, S. Owaki, and D.A. Shirley

October 1982

TWO-WEEK LOAN COPY

This is a Library Circulating Copy which may be borrowed for two weeks. For a personal retention copy, call Tech. Info. Division, Ext. 6782.

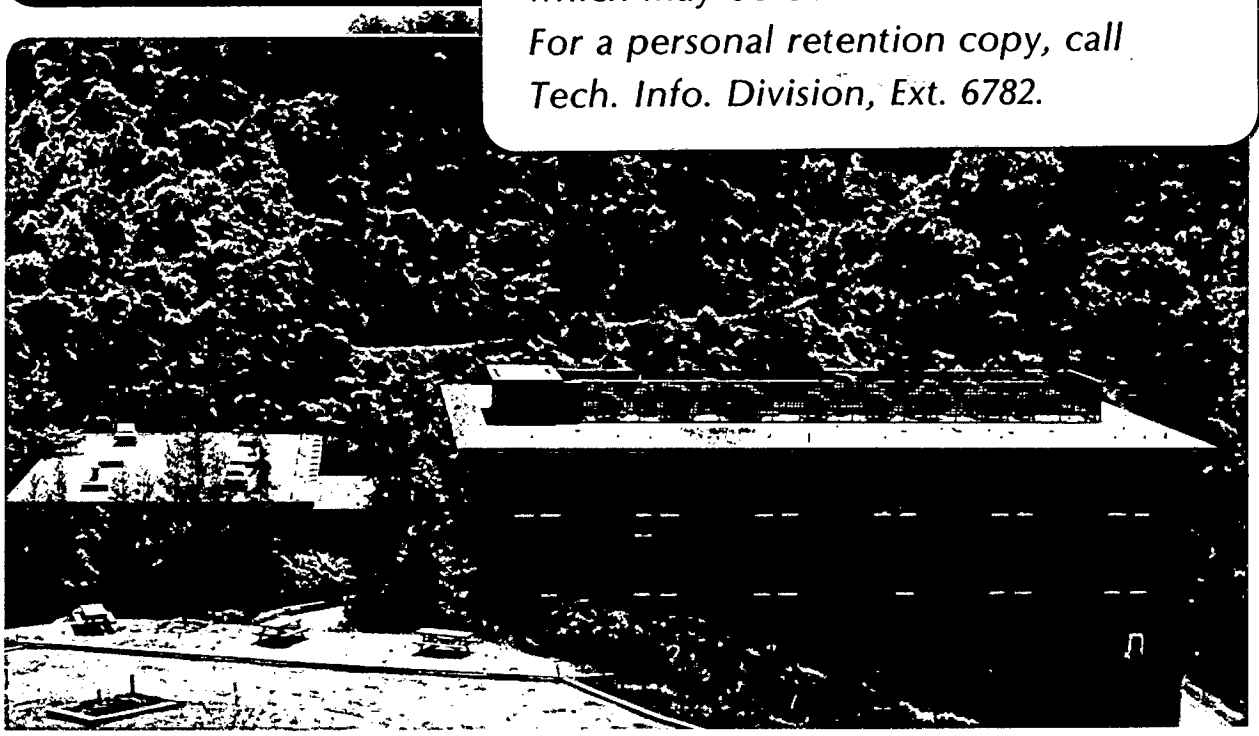

Prepared for the U.S. Department of Energy under Contract DE-AC03-76SF00098

LBL-13697 c.2

DISCLAIMER

This document was prepared as an account of work sponsored by the United States Government. While this document is believed to contain correct information, neither the United States Government nor any agency thereof, nor the Regents of the University of California, nor any of their employees, makes any warranty, express or implied, or assumes any legal responsibility for the accuracy, completeness, or usefulness of any information, apparatus, product, or process disclosed, or represents that its use would not infringe privately owned rights. Reference herein to any specific commercial product, process, or service by its trade name, trademark, manufacturer, or otherwise, does not necessarily constitute or imply its endorsement, recommendation, or favoring by the United States Government or any agency thereof, or the Regents of the University of California. The views and opinions of authors expressed herein do not necessarily state or reflect those of the United States Government or any agency thereof or the Regents of the University of California.

LBL-13697

ELECTRON SPECTROSCOPY STUDY OF INNER-SHELL PHOTOEXCITATION AND IONIZATION OF Xe

S. Southworth,* U. Becker,† C.M. Truesdale, P.H. Kobrin, D.W. Lindle, S. Owaki,‡ and D.A. Shirley

Materials and Molecular Research Division
Lawrence Berkeley Laboratory
and
Department of Chemistry
University of California
Berkeley, California 94720

ABSTRACT

Electron spectroscopy, combined with synchrotron radiation in the photon energy range $h\nu \simeq 60$–190 eV, was used to measure the angular distributions of Xe 5p and 5s photoelectrons and of $N_{4,5}OO$ Auger electrons. The branching ratios and partial cross sections for photoionization and Auger processes also were measured in certain cases. The measured asymmetry parameter β for 5p photoelectrons agrees well with many-electron calculations, which predict a pronounced oscillation in $\beta(5p)$ above the 4d ionization threshold due to the (4d,5p) intershell interaction. The $N_{4,5}OO$ Auger electrons are produced with photon-energy-dependent, anisotropic angular distributions, resulting from alignment of Xe^+ by photoionization. The theoretical analysis of Auger electron angular distributions is described, and theoretical calculations are found to predict

---

*Present address: Synchrotron Ultraviolet Radiation Facility, National Bureau of Standards, Washington, D.C. 20234
†Permanent address: Technische Universität Berlin, Fachbereich Physik, Berlin 12, Germany
‡Permanent address: Institute of Scientific and Industrial Research, Osaka University, Ibaraki, Osaka 567, Japan

the measured asymmetries well. In addition, Auger electron peaks were observed to broaden and shift at photon energies near the 4d ionization threshold because of post-collision interaction. The measured shifts of the $N_5O_1O_1$ $^1S_0$ line agree well with previous measurements and theory. Electron spectra recorded through the energy region of the 4d → np Rydberg states show that they decay primarily by the Auger process, while the 5p and 5s partial cross sections are relatively weakly affected by autoionization. However, distinct resonance structure was observed in the β parameters for $5p_{3/2}$ and $5p_{1/2}$ photoelectrons. The measured results are compared with a theoretical calculation of resonant photoionization for the 4d → 6p excitation.

I. Introduction

Several characteristic features of atomic inner-shell photoexcitation and ionization have been demonstrated in experimental and theoretical studies involving the 4d inner-subshell of Xe. These features have both one-electron character, directly involving transitions of 4d electrons, and many-electron character; i.e., intershell correlations with the 5p and 5s outer subshells and the Auger ionization of 4d-vacancy states. In this paper we report the results of a set of experiments involving Xe 4d photoexcitation and ionization, as obtained from photoelectron and Auger electron spectra recorded following excitation by synchrotron radiation.

Two sets of measurements of Xe electron spectra were performed. Selected early results from the first set were reported previously.[1] Additional results are given here. Fig. 1 of Ref. 1 showed an example of these spectra, which were recorded with a 5.3 Å (FWHM) monochromator bandpass. The 5p, 5s, and 4d photoelectron lines and the $N_{4,5}OO$ Auger spectrum were recorded in these measurements over the energy range $h\nu \simeq 70$–190 eV; i.e., from just above the 4d ionization threshold to near the 4d Cooper minimum.

In the second set of measurements, higher resolution over two smaller ranges of photon energy was employed. The $N_{4,5}OO$ Auger spectrum was recorded with a smaller monochromator bandpass (2.6 Å FWHM) and improved counting statistics over the range $h\nu \simeq 68$–82 eV, the energy region just above the 4d ionization threshold. Electron spectra were also recorded over the range $h\nu \simeq 60$–70 eV, to investigate resonant photoemission involving the $4d \rightarrow np$ Rydberg states.

Assuming pure electric-dipole photoabsorption of randomly oriented target atoms interacting with a linearly polarized photon beam, the differential photoionization cross section for each product channel (final ionic state plus photoelectron) can be expressed in the form[2]

$$\frac{d\sigma(\varepsilon)}{d\Omega} = \frac{\sigma(\varepsilon)}{4\pi}\,[1 + \beta(\varepsilon)\,P_2(\cos\theta)]. \qquad (1)$$

Here $\sigma(\varepsilon)$ is the angle-integrated partial cross section, $P_2(\cos\theta)$ is a Legendre polynomial, equal to $(1/2)(3\cos^2\theta - 1)$, θ is the angle between the photoelectron momentum direction and the photon polarization direction, ε is the photoelectron energy, and $\beta(\varepsilon)$ is the photoelectron asymmetry parameter, having the restricted range $-1 \leq \beta(\varepsilon) \leq 2$. Conservation of angular momentum and parity similarly restrict the angular distributions of Auger electrons to the form of Eq. (1), when they are ejected following electric-dipole photoemission.[3] Thus, the angular distributions of photoelectrons and Auger electrons are completely described by the single parameter $\beta(\varepsilon)$, in the dipole approximation. This approximation is quite good at low photon energies, but at higher energies (generally, several hundred eV) a more complicated form of the angular distribution can result due to the contributions of additional multipole components.[4] In our previously reported[1] and present work, spectra were recorded using photon energies $h\nu \leq 330$ eV, and the measurements are

interpreted using Eq. (1); i.e., the dipole approximation is assumed to be valid.

The photoabsorption cross section of Xe displays a strong, broad maximum centered near 100 eV and a weaker, very broad maximum between 200 and 500 eV.[5-7] These features have been attributed to a shape resonance (arising from an effective potential barrier) and a Cooper minimum in the $4d \rightarrow \varepsilon f$ photoemission cross section.[8-10] Previously, we reported measurements of the asymmetry parameter $\beta(\varepsilon)$ over $h\nu \simeq 70$-330 eV for 4d photoelectrons.[1] In good agreement with theoretical calculations (for example, Ref. 10), the $\beta(4d)$ parameter was observed to oscillate strongly as a function of energy, due to the shape resonance and Cooper minimum in the $4d \rightarrow \varepsilon f$ channel.

The central-field[9] and Hartree-Fock[10] calculations indicate that 4d photoemission dominates the total photoionization cross section of Xe over the energy range from the 4d ionization threshold ($h\nu \simeq 68$ eV) to the 3d threshold ($h\nu \simeq 680$ eV). Subsequently, many-electron photoionization calculations[11-14] and photoelectron spectroscopic measurements[15-18] demonstrated that the outer-shell 5p and 5s photoemission processes are affected by electron-correlation interactions with the 4d subshell, both above and below the 4d ionization threshold (for reviews, see Refs. 11, 13, and 19). In this paper we report measurements of the asymmetry parameter $\beta(\varepsilon)$ for 5p photoelectrons over the energy region of the shape resonance in the 4d cross section. Our measurements agree with and extend those of Refs. 16 and 18 and confirm a pronounced interchannel-coupling effect predicted theoretically.[12-14]

Photoemission from the Xe 4d subshell produces an excited ionic state which lies energetically above the double-ionization threshold. Thus, the Xe^+ ($4d^{-1}$) vacancy state can decay by ejection of secondary Auger electrons. Our previous measurements[1] confirmed theoretical predictions[20,21] that Xe $N_{4,5}OO$ Auger electrons are produced with photon-energy-dependent, anisotropic angular distributions, due to alignment of Xe^+ by photoionization. Theoretical analysis shows that the alignment and subsequent Auger electron angular distribution provide a measure of the ratio

$$\gamma(\varepsilon) = \sigma(4d \rightarrow \varepsilon p)/\sigma(4d \rightarrow \varepsilon f) \qquad (2)$$

of the partial cross sections for 4d photoemission into p- and f-waves. Thus, the Auger electron asymmetry yields information on the photoionization process which is complementary to that determined by the partial photoionization cross section and the photoelectron angular distribution.

Schmidt and co-workers[22] have observed an asymmetric broadening and energy shifts of Xe N_5OO Auger electron peaks produced following photoionization at photon energies near the 4d ionization threshold. These effects are attributed to a type of final-state correlation called post-collision interaction (PCI). Here we report the results of an additional set of Xe $N_{4,5}OO$ Auger spectra recorded near and just above the $4d^{-1}$ threshold, where PCI effects are observed and Auger electron asymmetries are relatively large. The $N_5O_1O_1$ $^1S_0$ line was observed to broaden and

shift as a function of photon energy, in good agreement with the measurements of Schmidt et al.[22] and the theoretical model of PCI developed by Niehaus.[23] The measured asymmetry parameters for the Auger electrons agree well with theoretical values[21] based on Hartree-Fock calculations of the partial-wave branching ratio $\gamma(\varepsilon)$.

A prominent series of 4d $\rightarrow$ np Rydberg excitations has been recorded in photoabsorption spectra over the energy range $h\nu \approx 65$–70 eV.[24,25] Because of the effective potential barrier for $\ell = 3$ angular momentum, the 4d $\rightarrow$ nf Rydberg series is not observed. Several continuum channels are available for the decay of the np-resonant states. Resonant Auger decay competes with the 5p and 5s primary continuum channels. We have recorded electron spectra through the resonant photon energy region (4d-resonance spectra have been reported previously in Refs. 22, 26, and 27). Though the present spectra were recorded with a monochromator bandpass (0.4–0.6 eV FWHM) which is large compared with the resonance linewidths (~0.1 eV), certain strong qualitative features were observed. As expected, based on the photoabsorption lineshape analysis,[25] the 4d-excited resonances decay predominantly by the Auger process, and the 5p and 5s partial cross sections appear relatively unaffected by autoionization. However, pronounced resonance structure appears in the asymmetry parameters $\beta(\varepsilon)$ for $5p_{3/2}$ and $5p_{1/2}$ photoelectrons. In contrast, the 5s photoelectrons are produced with large asymmetries $\beta \approx 1.8$–2.0, and no resonance structure was observed. We compare the observed resonance effects on 5p and 5s photoemission with a theoretical calculation.[29] The comparison suggests the necessity of including the Auger decay channels in theoretical models of inner-shell resonant photoexcitation.

II. Experimental Methods

The measurements were made at the Stanford Synchrotron Radiation Laboratory (SSRL) on Beam Line III-1, which employs the grazing-incidence "grasshopper" monochromator.[30] An aluminum window was used to separate the gas-phase electron spectrometer from the ultra-high vacuum of the monochromator and beam line.[31] We estimate a high degree of linear polarization (~98%) for this beam line over the energy range of the measurements, based on the large asymmetry ($\beta = 1.94$) measured for Ag 4s $\rightarrow \varepsilon p$ photoelectrons with a rotatable analyzer on a similar XUV beam line at SSRL.[32] The limiting value for this transition is $\beta = 2$. If the observed $\beta < 2$ results only from incomplete polarization of the photon beam, a value of 98% linear polarization is still indicated. It was demonstrated in a previous publication[33] that because of calibration procedures described below, our derived β values are quite insensitive to the precise value of the photon polarization P over a wide range ($P \simeq 70 - 100\%$).

As described in Ref. 31, the time structure of the synchrotron radiation was used to record time-of-flight (TOF) spectra of photoelectrons and Auger electrons. Two TOF detectors were operated simultaneously, one positioned at the "magic angle" ($\theta = 54.7°$) with respect to the polarization vector, and the other at $\theta = 0°$. A detailed description of this double-angle-TOF method was given in a recent publication.[33] Asymmetry parameters β are determined from the relative intensities of photoelectrons recorded at the two ejection angles. The instrument was calibrated for angular distribution measurements, as a function of

electron energy ε, by recording photoelectron lines having known $\beta(\varepsilon)$ values. The relative collection efficiency $f_0(\varepsilon)$ of the two detectors is given by [33]

$$f_0(\varepsilon) = \frac{N_c(0^\circ,\varepsilon)/N_c(54^\circ,\varepsilon)}{1 + \beta_c(\varepsilon)} , \tag{3}$$

where $N(\theta,\varepsilon)$ is the number of photoelectron counts recorded at detector angle θ, and the subscript c represents the calibration gas. In the present experiments, the Ne 2p photoelectron line was used for calibration, because its $\beta(\varepsilon)$ value has been accurately determined over a large energy range.[34] An example of a calibration curve is plotted in Fig. 1 along with the Ne 2p $\beta(\varepsilon)$ curve. The unknown $\beta(\varepsilon)$ values of Xe were then determined from the relation

$$\beta_0(\varepsilon) = -1 + \frac{N(0^\circ,\varepsilon)/N(54^\circ,\varepsilon)}{f_0(\varepsilon)} . \tag{4}$$

The $\beta_0(\varepsilon)$ values given by Eq. (4) were corrected (by less than 0.05 β unit) to account for incomplete polarization of the photon beam and for angle-averaging over the interaction volume and collection solid angles of the detectors. We emphasize that the calibration procedure greatly reduces the effects of certain experimental systematic errors by enfolding

them into the calibration function $f_0(\epsilon)$ (a full discussion of this point is given in Ref. 33). We estimate systematic errors to be ± 0.10 β unit or less.

The magic-angle TOF spectra, which are independent of $\beta(\epsilon)$ values, were used to determine relative partial cross sections and branching ratios. The relative transmission of the magic-angle detector was determined as a function of electron energy by using the photoelectron spectra of the Ne 2p line, for which the partial photoionization cross section is tabulated.[34] The photon beam intensity was monitored with a sodium salicylate scintillator, phototube, and picoammeter. The sample gas density was monitored using a capacitance manometer on the gas inlet system.[31]

III. 4d and 5p Photoelectron Asymmetries

In the first set of spectra recorded over $h\nu \approx 70$–190 eV with a 5.3 Å bandpass, photoelectrons from the individual fine structure levels of the 4d and 5p subshells were not resolved. A photoelectron peak at a low TOF (high kinetic energy) was identified as arising from 4d photoelectrons produced by second-order light. The second-order photolines were used to extend the $\beta(4d)$ measurements beyond the Cooper minimum. Good agreement was obtained between $\beta(4d)$ values given by second-order light with values given by first-order light at energies $h\nu \approx 130$–190 eV where the two sets of measurements overlapped. The $\beta(4d)$ results were plotted in Ref. 1 and discussed there in comparison with theoretical calculations.

In Fig. 2 are plotted the measured $\beta(5p)$ values along with previous measurements[16,18,35] (see Ref. 36) and two theoretical curves based on the random-phase approximation with exchange (RPAE).[12,13] The RPAE is nonrelativistic but can include electron correlations.[11] The dashed theoretical curve includes the 5p intrashell correlations only, while the solid curve also accounts for intershell correlation with the 4d subshell. The data clearly support the theoretical interpretation of a strong intershell correlation (or interchannel coupling) effect on $\beta(5p)$. In this correlation process the 4d subshell undergoes virtual photo-excitation, with the excitation passing to the 5p subshell via Coulomb interaction. The interchannel coupling produces a prominent oscillation in $\beta(5p)$ in the energy region of the delayed maximum in the 4d photoionization cross section. The full oscillation is observed

experimentally in the present measurements. Other theoretical calculations which, respectively, do[14,37] and do not[10,38] include interchannel coupling with the 4d subshell give $\beta(5p)$ results similar to the full and dashed curves in Fig. 2.

IV. $N_{4,5}OO$ Auger Electron Angular Distributions

The Auger effect is usually treated as a two-step process, in which the decay of the inner-vacancy state is considered independent of the excitation process. In the present experiments, excitation was produced by photoemission from the 4d subshell:

$$h\nu + Xe(4d^{10}5s^{2}5p^{6}\ {}^{1}S_{0}) \rightarrow Xe^{+}(4d^{9}5s^{2}5p^{6}\ {}^{2}D_{3/2,5/2}) + e^{-} \quad . \qquad (5)$$

In the subsequent decay process, a 5p or 5s electron fills the 4d hole, and a second O-shell electron is ejected. Flügge et al.[20] showed that photoemission from an atomic subshell with $j > 1/2$ produces an aligned vacancy state if its total angular momentum J also exceeds 1/2. As a result, the Auger electrons should exhibit anisotropic angular distributions. As reported previously,[1] this effect was confirmed in our first set of Xe $N_{4,5}OO$ Auger spectra. The measured Auger electron asymmetries varied with photon energy, in good qualitative agreement with the calculations of Berezhko et al.[21] for the alignment of Xe^{+} $(4d^{-1})$ by photoionization. To our knowledge, no experimental observation of this effect had been made previously, although anisotropic angular distributions of Auger electrons had been measured following inner-shell ionization by electron impact.[39] Here we report additional results based on our (lower resolution) first set of Auger spectra, and then give the

results of an additional set of spectra which allow a more quantitative comparison with theory. First we give a summary of the theoretical analysis of Auger electron angular distributions.

A. Theoretical Background

Consider an ensemble of atomic ions, all in the same inner-shell vacancy state with total angular momentum J. The subsequent Auger electron angular distribution depends, at least in part, on the distribution of the ensemble over magnetic sublevels JM. The angular symmetry properties of the ensemble are described quite generally by use of the density matrix[40] and its statistical tensors[41] or "state multipoles" T_{KQ}. Surveys of these topics are given, for example, in Refs. 42 and 43. The statistical tensors formulation is particularly advantageous for the description of successive radiations--in the present case, Auger emission following photoemission.

Prior to the photoemission step, the target atoms are randomly oriented. Thus, the atomic density matrix is spherically symmetric and only the monopole term T_{00} is nonzero. Photoabsorption by a dipole process can introduce statistical tensors of rank $K \leq 2$. With the use of a linearly-polarized photon beam, the natural choice for a quantization axis is parallel to the polarization vector, because the photoexcited system has axial symmetry about that direction. In addition, the photoexcited system is symmetric with respect to reversal of the quantization axis. As a result of axial symmetry, the density matrix is diagonal, and the ensemble has the properties, statistically, of an incoherent super-

position of magnetic substates JM. In the present example, the populations of the magnetic sublevels are proportional to the partial photoionization cross sections $\sigma(JM)$. Symmetry with respect to reversal of the quantization axis implies that the sublevels M and -M are equally populated, i.e., $\sigma(J-M) = \sigma(JM)$. With these symmetry conditions, all of the spherical tensor components vanish except T_{00} and T_{20}. As a consequence, the angular distributions of photofragments take the form of Eq. (1), that is, $I(\theta) \propto 1 + \beta P_2(\cos\theta)$, where θ is measured with respect to the photon polarization vector and β is an "asymmetry parameter".

Auger electron angular distributions are conveniently described by defining the "alignment tensor" A_{20}:[20,21]

$$A_{20}(J) = T_{20}(J)/T_{00}(J)$$

$$= \frac{\sum_M (-1)^{J-M}(JMJ-M|20)\sigma(JM)}{\sum_M (-1)^{J-M}(JMJ-M|00)\sigma(JM)}$$

$$= \left[\frac{5}{J(J+1)(2J+3)(2J-1)}\right]^{1/2} \frac{\sum_M [3M^2-J(J+1)]\sigma(JM)}{\sum_M \sigma(JM)} \qquad (6)$$

where $(JMJ-M|KQ)$ is a Clebsch-Gordon coefficient. Thus, for an ensemble of Xe^+ $^2D_{5/2}$ ions produced by photoemission, the alignment can be expressed as

$$A_{20}(5/2) = \frac{1}{\sqrt{14}} \left[\frac{5\sigma(\frac{5}{2}\,\frac{5}{2}) - \sigma(\frac{5}{2}\,\frac{3}{2}) - 4\sigma(\frac{5}{2}\,\frac{1}{2})}{\sigma(\frac{5}{2}\,\frac{5}{2}) + \sigma(\frac{5}{2}\,\frac{3}{2}) + \sigma(\frac{5}{2}\,\frac{1}{2})} \right] \quad . \tag{7}$$

Similarly, photoemission from the $4d_{3/2}$ subshell produces an aligned system of $Xe^{+}\ {}^{2}D_{3/2}$ ions described by

$$A_{20}(3/2) = \frac{\sigma(\frac{3}{2}\,\frac{3}{2}) - \sigma(\frac{3}{2}\,\frac{1}{2})}{\sigma(\frac{3}{2}\,\frac{3}{2}) + \sigma(\frac{3}{2}\,\frac{1}{2})} \quad . \tag{8}$$

When the magnetic sublevels JM are unequally populated, T_{20} and A_{20} are nonzero, in general, and the system is said to be "aligned".

The asymmetry parameter β for a particular Auger transition is proportional to the alignment tensor of the initial state in the transition:

$$\beta(\varepsilon) = \alpha A_{20}(\varepsilon), \tag{9}$$

where α depends on transition matrix elements of the Coulomb operator and on the phases of the partial waves which describe the ejected Auger electron.[44,45] In Eq. (9), ε represents the photoelectron kinetic energy. In the two-step model, the energy dependence of the Auger electron asymmetry is determined only by the energy dependence of the

alignment tensor. For a given Auger transition, the Coulomb matrix elements and continuum wave phases are fixed, so α is independent of photon energy. $A_{20}(\varepsilon)$ is a property of a given inner-shell vacancy state, while the factor α is determined by the Auger decay step and varies among the Xe^{2+} final states. According to Eq. (9), the asymmetry parameters of all Auger transitions produced from the same inner-shell vacancy should display the same photon-energy dependence, but may differ in magnitude by constant scale factors.

For the case of a Xe^{2+} final state having total angular momentum $J_f = 0$, there is a single continuum wave, and the Auger electron angular distribution is then independent of the Coulomb matrix element and phase shift.[44] The factor α is then given by a product of angular momentum coupling coefficients[45] (see Ref. 46). In particular, consider the case that the final states of the $N_{4,5}OO$ Auger transitions are $^1S_0$ states:

$$Xe^+(4d^9 5s^2 5p^6\ {}^2D_J) \rightarrow Xe^{2+}({}^1S_0) + e^-(\varepsilon d_J),\ J = 3/2,\ 5/2. \qquad (10)$$

The decay factors α are calculated[45,46] to give the following expressions for the Auger electron asymmetry parameters:

$$\beta(N_5OO\ ^1S_0) = 4\sqrt{\frac{2}{7}}\,A_{20}(5/2) \tag{11}$$

$$\beta(N_4OO\ ^1S_0) = 2A_{20}(3/2). \tag{12}$$

Thus, measurement of the asymmetry parameters for these Auger transitions provides a direct determination of the alignment tensors.

The analysis of Flügge et al. shows that A_{20} should always be nonzero for the case of photoemission from an atomic subshell with $j > 1/2$ and for which the ionic state formed has total angular momentum $J > 1/2$. The value of A_{20} is determined by the magnitudes of the photoionization matrix elements. In the nonrelativistic limit, a 4d electron can be photoemitted into two dipole-allowed continuum waves: εp and εf. Theoretical analysis[20,21] shows that A_{20} is determined by the partial-wave branching ratio, Eq. (2). Specifically, Berezhko et al.[21] showed that the alignment tensor can be expressed as

$$A_{20} = C\left[\frac{1 + a\gamma}{1 + \gamma}\right] , \tag{13}$$

where γ is the energy-dependent ratio defined in Eq. (2), and C and a are constants determined by angular momentum coupling coefficients. For $Xe^+\ ^2D_{5/2}$, $a = 7/2$ and $C = (1/5)(2/7)^{1/2}$; for $Xe^+\ ^2D_{3/2}$, $a = 7/2$ and $C = 1/10$.

In an independent-electron model, the photoionization cross sections are determined by the radial dipole matrix elements $R_{n\ell,\varepsilon\ell\pm1}$

(Ref. 10). Thus, in the present example, the partial-wave branching ratio can be expressed as

$$\gamma(\varepsilon) = (2/3)R^2_{4d,\varepsilon p}/R^2_{4d,\varepsilon f} \quad . \tag{14}$$

Berezhko et al.[21] have calculated $A_{20}(\varepsilon)$ for Xe^+ $(4d^{-1})$ using both Herman-Skillman and Hartree-Fock wave functions. An energy-dependent alignment is predicted, arising from the centrifugal barrier and Cooper minimum in the $4d \rightarrow \varepsilon f$ channel. These are the same factors that produce oscillations in the 4d photoelectron asymmetry.[1]

Manson has provided us with a tabulation of Hartree-Fock photoionization calculations for the Xe 4d subshell, which were reported in Ref. 10. These calculations provide the partial-wave branching ratio $\gamma(\varepsilon)$. This parameter is listed in Table I along with the resulting value of $A_{20}(\varepsilon)$ for Xe^+ $^2D_{5/2}$ calculated using Eq. (13). Results are given for both the length and velocity forms of the dipole operator. The values of $A_{20}(\varepsilon)$ listed in Table I are similar to the Hartree-Fock results given in a graph in Ref. 21. Also listed in Table I are the resulting theoretical values (Eq. (11)) for the Auger electron asymmetry parameter β for the case of a transition of the type N_5OO $^1S_0$. A corresponding table of $A_{20}(\varepsilon)$ and $\beta(N_4OO\ ^1S_0)$ for Xe^+ $^2D_{3/2}$ can be obtained using Eqs. (12) and (13) and the values of $\gamma(\varepsilon)$ listed in Table I.

B. Lower Resolution Results

From the set of Xe spectra recorded over $h\nu \approx 70$–190 eV, asymmetry parameters β were determined for the Auger electron peaks numbered 1–4 in Fig. 1 of Ref. 1. The Auger spectrum was identified by comparison with the spectrum recorded and analyzed by Werme et al.[47] The Auger lines numbered 1 and 3 are produced, respectively, by the two transitions

$$Xe^{+}(4d^{9}5s^{2}5p^{6}\ {}^{2}D_{5/2}) \rightarrow Xe^{2+}(4d^{10}5s^{0}5p^{6}\ {}^{1}S_{0}) + e^{-} \tag{15}$$

$$Xe^{+}(4d^{9}5s^{2}5p^{6}\ {}^{2}D_{5/2}) \rightarrow Xe^{2+}(4d^{10}5s5p^{5}\ {}^{1}P_{1}) + e^{-} \quad . \tag{16}$$

(This assignment of line number 1 (Eq. (15)) differs from that given in Ref. 47; assignments will be discussed below as the second set of Auger spectra are presented.) To reduce scatter in the data, particularly at high photon energies, some of the β values derived from these lower-resolution spectra represent an average over two or three measurements obtained at nearby photon energies. The results are plotted in Fig. 3 along with theoretical curves for an Auger transition of the general type $N_5 00\ {}^{1}S_0$. Thus, the measured β values for the $N_5 0_1 0_1\ {}^{1}S_0$ transition can be directly compared with the theoretical curves. The same alignment tensor $A_{20}(\varepsilon)$ is appropriate for describing the $N_5 0_1 0_{2,3}\ {}^{1}P_1$ transition, but the Auger decay (coefficient) α might differ from that of Eq. (15).

In Fig. 3, the data qualitatively follow the predicted energy variation of the Auger electron asymmetry parameter. Eqs. (2),(9), and

(13) show that the alignment is relatively strong, so that the Auger asymmetry is relatively large, where the $4d \rightarrow \varepsilon f$ photoemission transition strength is small relative to that of $4d \rightarrow \varepsilon p$. Thus, relatively large Auger asymmetries are produced near the 4d ionization threshold, where $\sigma(4d \rightarrow \varepsilon f)$ is small due to the centrifugal barrier in the f-wave effective potential. The f-wave channel quickly becomes predominant as the potential barrier is surpassed, so that smaller β(Auger) values are produced over the energy range $\varepsilon \approx 10$-100 eV. Then, relatively large Auger asymmetries are produced again near the Cooper minimum in the f-wave channel. Berezhko and co-workers extended their theoretical studies of alignment by using RPAE calculations to include the effects of many-electron correlations and electron shell rearrangement.[49] In the case of Xe^+ $(4d^{-1})$, the inclusion of these interactions produced a moderate shift in the energy position of the Cooper minimum feature, in comparison with the Hartree-Fock calculation, but did not alter the general form of $A_{20}(\varepsilon)$.

Figure 3 shows that the measured β values of the $N_5O_1O_1$ $^1S_0$ transition are in reasonably good agreement with theory, and that, at lower energies, $\beta(N_5O_1O_{2,3}\ ^1P_1) < \beta(N_5O_1O_1\ ^1S_0)$. The latter result could be due to differing decay factors α. However, it will be seen that the higher resolution set of β(Auger) measurements obtained just above the 4d ionization threshold are somewhat higher than the first results plotted in Fig. 3, and that no variations are observed among different Auger transitions. These results are to be preferred,

primarily for the following reasons. Though the signal-to-background was not greatly improved, the second set of spectra were obtained with superior counting statistics, particularly near the 4d ionization threshold. For both sets of spectra, background subtraction was an important factor in determining the relative areas of the 0° and 54.7° peaks (and hence in determining β). Thus, errors in background subtraction could create discrepancies. The second set of TOF spectra were recorded with a smaller time window which covered only the kinetic energy range of the Auger electrons. This gave more collection channels per nsec and an effectively better resolution of the $N_{4,5}O_1O_{2,3}\ ^1P_1$ Auger peaks. Also, the first spectra were recorded with a much larger photon bandpass (5.3 Å FWHM; 2 eV at $h\nu$ = 70 eV) than the second spectra (2.6 Å FWHM; 1 eV at $h\nu$ = 70 eV). Some other factors which could in principle create a discrepancy, such as second-order light and uncertainty in the calibration of the energy scale of the monochromator, appear not to be significant. In short, we regard the first results (Fig. 3) to be qualitatively correct but prefer the higher resolution results for a quantitative comparison with theory.

Before discussing the second set of Auger spectra and results, we give an additional result obtained from the first set of spectra. The branching ratio $N_5OO:N_4OO$ between Auger lines produced by transitions of N_5 and N_4 core holes to the same Xe^{2+} final state is plotted in Fig. 4. This branching ratio was determined for the two pairs of lines $N_{4,5}O_1O_1\ ^1S_0$ and $N_{4,5}O_1O_{2,3}\ ^1P_1$. No strong variations were observed between the two sets of branching ratios, and the average values are given in order to

reduce the scatter in the measurements. Also plotted in Fig. 4 are a theoretical curve[50] and experimental data[51-53] for the $4d_{5/2}:4d_{3/2}$ photoelectron branching ratio itself. The Auger electron branching ratio closely follows the corresponding photoelectron branching ratio. This is the result expected if no variation occurs between the decay patterns for the two fine structure vacancy states, i.e., a variation in the branching ratios for transitions to the various Xe^{2+} final states.

C. Assignment of the Auger Electron Spectrum

Figure 5 shows an example from the second set of 0° and 54.7° TOF spectra of the Xe $N_{4,5}OO$ Auger electrons. Spectra were recorded over the energy range $h\nu$ = 67.7-81.9 eV with a monochromator bandpass of 2.6 Å FWHM. Since the Auger electron energies are independent of $h\nu$, there are contributions to the Auger peaks arising through excitation by second- and higher-order diffracted light and by scattered light in the photon beam. These contributions could of course interfere with the measurements of the Auger electron asymmetry parameters and branching ratios to an extent that will depend on the relative intensities of the components of the photon beam and on the relative photoionization cross section of the 4d subshell at the component photon energies. We determined the order-composition of the photon beam over the energy region of the Auger spectra by recording 54.7° TOF spectra of Ne. Dividing the intensities of the first- and higher-order photolines of Ne by the corresponding photo-ionization cross section[34] yields the relative intensities of the

order-components of the photon beam. Scattered light appeared to be insignificant in this energy range. From the order-composition of the photon beam and the relative photoionization cross section of the Xe 4d subshell,[54] we estimate that the first-order light contributed about 95% of the Auger electron signal in our spectra. Therefore, higher-order light contributions to the results appear negligible.

Not shown in Fig. 5 are the $N_{4,5}O_{2,3}O_{2,3}$ Auger lines which were unresolved in our TOF spectra due to their higher kinetic energies and closer spacings. Only the lower energy, intense lines numbered 1-7 in Fig. 5 were analyzed for asymmetry parameters and branching ratios. Some of these lower energy Auger lines, which result from transitions to higher energy levels of Xe III, have not been definitively assigned. Good correspondence was obtained between the present spectra and the high-resolution spectrum recorded by Werme et al.[47] using electron impact excitation, allowing comparison with their assignments. The $N_{4,5}$-$O_{2,3}O_{2,3}$ and -$O_1O_{2,3}$ series of lines were assigned by Werme et al. by comparison with the spectroscopically observed[55] levels of Xe III. Thus, lines 1 and 2 in Fig. 5 are the $N_{4,5}$-pair identified with the final state $5s5p^5\ {}^1P_1$. Lines 3,5 and 6,7 are also $N_{4,5}$-pairs. Werme et al. used the Moore tables[55] to identify line 4 as the N_5 line produced by Auger decay to the final state $5s^25p^3({}^2P)6s\ {}^1P_1$. Hence, this line was termed a satellite, to be regarded as originating from shake-up in the Auger process. However, the $N_{4,5}$-pairs 3,5 and 6,7 could not be assigned using Ref. 55, because they are produced by final states at

higher energies than those reported in the spectroscopic tables. One of these two pairs of lines should be the $N_{4,5}O_1O_1$ lines and the other, presumably, satellites. Thus, since the $5s^05p^6$ level had not been observed spectroscopically, and because intense satellite lines are also present in the Auger spectrum, the $N_{4,5}O_1O_1$ lines could not be identified with certainty by Werme et al. A similar situation was obtained in the analogous case of the $M_{4,5}NN$ spectrum of Kr, which was also reported in Ref. 47. By comparison with assignments of the corresponding ns^0np^6 final states in Kr and the other rare gases,[56] Werme et al. assigned lines 3 and 5 in Fig. 5 as $N_{4,5}O_1O_1\ {}^1S_0$. By comparison also with the Kr $M_{4,5}NN$ spectrum, the lowest energy lines 6 and 7 were attributed to the satellite final state $5s^25p^3(^2P)7s\ {}^1P_1$.

Subsequently, the theoretical studies of Larkins and of McGuire[57] indicated that the $M_{4,5}N_1N_1$ transitions in Kr should be reassigned as the lowest energy intense lines, which previously were identified as satellites. Similarly, the Xe $N_{4,5}OO$ Auger-electron energies calculated semiempirically,[58] i.e., using experimental binding energies and Hartree-Fock values for Slater integrals, indicate that lines 6 and 7 in Fig. 5 should be identified as $N_{4,5}O_1O_1\ {}^1S_0$, and this is the assignment that we adopt. This revised assignment appears also to have been adopted in Ref. 26 for the corresponding resonant-Auger spectrum, and is supported by results of electron impact studies of VUV-emission from Xe III levels.[59]

This leaves lines 3 and 5 still to be reassigned. We propose that they be identified as satellites associated with the $5s5p^5\ ^1P_1$ primary configuration, i.e., satellites of the $N_{4,5}O_1O_{2,3}\ ^1P_1$ lines (1 and 2). It seems likely that all of the lines between the $N_{4,5}$-pairs 1,2 and 6,7 are of this origin. This proposed identification is based on the corresponding case of the $Xe^+\ 5s5p^6\ ^2S_{1/2}$ photoline with its associated set of intense satellites observed in photoelectron spectra (see, for example, Refs. 60 and 61). The $5s5p^6$ satellites occur in the energy region of the $5s^25p^4(SL)n\ell$ levels[55] (note that Hansen and Persson[62] have given revised identifications of these levels). Theoretical studies[61-64] indicate that the $5s5p^6$ satellites arise primarily through correlation processes which can be described as final ionic state configuration interaction (FISCI).[65] The FISCI mechanism requires that the satellite lines arise from states that have the same total angular momentum and parity as the primary ionic configuration $5s5p^6\ ^2S_{1/2}$. Hence, Hansen and Persson[62] have assigned the satellites to even parity states of the type $5s^25p^4(SL)nd$ and $5s^25p^4(SL)ns$ which have total angular momentum J = 1/2. The primary and satellite LSJ configurations become strongly mixed by electron correlation, so it is not entirely accurate to label the observed levels with a particular configuration.[62,64] A detailed description of the origin of these satellites might involve a combination of types of many-electron interactions;[61,63] however, the FISCI mechanism appears to be the dominant process.

We propose that the satellite lines in the Xe $N_{4,5}OO$ Auger spectrum result correspondingly from interaction among the Xe^{2+} configurations $5s5p^5$, $5s^25p^3(SL)nd$, and $5s^25p^3(SL)ns$ with total angular momentum J = 1. The most intense satellites of Xe^+ $5s5p^6$ are due to the $5s^25p^45d$ and $5s^25p^46d$ configurations, and the $5s^25p^4ns$ contributions appear to be less important.[61-64] Hansen and Persson[62] identify the strongest satellite with the level $5s^25p^4(^1D)5d\ ^2S_{1/2}$, which lies at 5.48 eV higher binding energy than the primary line $5s5p^6\ ^2S_{1/2}$. The strongest $N_{4,5}$-pair of satellites in the Auger spectrum (lines 3 and 5) also lie at 5.5 eV from the primary lines 1 and 2. Therefore we tentatively identify lines 3 and 5 with the final state $5s^25p^3(^2P)5d\ ^1P_1$. As mentioned above, line 4 was originally identified with the final state $5s^25p^3(^2P)6s\ ^1P_1$, by comparison with the spectroscopic data.[55] However the table of the corresponding $5s^25p^4n\ell$ levels of Xe II has been reassigned,[62] and similar reassignments may apply to the table of Xe III levels. We consider line 4 also to be a satellite originating from the N_5 core hole, but leave the final state unassigned. The present assignments of lines 1-3 and 5-7 are listed in Table II.

We note that the proposed $5s5p^5 \rightarrow 5s^25p^3n\ell$ excitation in Xe III is one more example of a rather general phenomenon which has been observed by photoelectron spectroscopy in a wide variety of systems--namely, electron-pair excitation from an outer valence shell in the presence of a hole in an inner valence shell. This kind of excitation is energetically favored because the pair of electrons are excited into a higher- and a

lower-energy orbital (in contrast to correlations in systems with filled inner subshells). Thus the correlation is very strong and the resulting "satellites" intense.

In the above discussion, we have proposed only that the satellite lines in the Auger spectrum arise from final state configuration mixing, in analogy with the FISCI satellites of the 5s photoline. However, other types of electron correlation mechanisms may also be important, such as those described by initial state configuration interaction (ISCI).[65] In the ISCI mechanism, pair-excited configurations of the type $4d^9 5s^2 5p^4 nd^2\ {}^2D$ could contribute to the initial state of the Auger process. These $5p^2 \rightarrow nd^2$ configurations in the initial state provide an additional mechanism for populating satellites in the final state.[66] Theoretical studies are needed both to confirm and to quantify the proposed identification of the Auger satellite lines. It appears that this would provide an interesting system for theoretical study of electron correlation.

D. Higher Resolution Results

The 54.7° TOF Auger spectrum recorded at $h\nu$ = 67.7 eV is shown in Fig. 6. This photon energy lies just above the $4d_{5/2}$ ionization threshold (67.55 eV), but below the $4d_{3/2}$ threshold (69.52 eV); actually, $h\nu$ lies in between the n = 6 and 7 members of the $4d_{3/2} \rightarrow np$ Rydberg series.[24] Since the N_4 vacancy in Xe^+ is not produced at this energy, only the N_5OO Auger lines appear in the spectrum. Comparison with Fig. 5 indicates a slight shift of the Auger lines to

smaller TOF (higher kinetic energy) and a broadening. These effects are attributed to the post-collision interaction (PCI) among the photoelectron, Auger electron, and atomic ion following near-threshold photoionization.[22]

Because of the nonlinear variation of the energy scale in a TOF spectrum (see Fig. 5), the shift and broadening are most noticeable for the lowest energy line, number 7, which we have assigned as $N_5O_1O_1\ ^1S_0$. In Fig. 7 are plotted the 54.7° TOF spectra of line 7 recorded just above the $4d_{5/2}$ ionization threshold and at 14.4 eV above threshold. The broadening and shifting of the line are readily apparent in this comparison.

It should be explained how we obtained the kinetic energy scales given with the TOF spectra in Figs. 5 and 7. The spectra are recorded with a fixed time scale, i.e., a constant number of collection channels per nsec, which is determined using a delay generator to calibrate the timing circuit with known time intervals. To convert the channel numbers to an actual TOF scale, the channel corresponding to TOF = 0 nsec is found. This channel can be obtained from the prompt signal (TOF ≃ 1 nsec) Rayleigh scattering of the photon beam by the sample gas.[31] If a prompt signal is not recorded, the TOF = 0 channel is determined as a fitting parameter. Each collection channel in the TOF spectrum can then be converted to the corresponding kinetic energy, by use of the path length between the source region and the detector. The path length is always known to within a few percent, and the actual value used for energy conversion is adjusted slightly to best fit the peak positions to known

kinetic energies. In Table II are listed the kinetic energies of the Auger lines determined by energy conversion of the TOF spectrum in Fig. 5. The energy-converted values agree well with the measurements of Werme et al.

The point to be emphasized here is that the TOF spectra can be used to measure small energy shifts, such as those due to the PCI effect. Table II shows that a fairly accurate energy conversion was obtained over a range of about 13 eV. Small energy shifts, amounting to a few percent of this range, are readily determined. For the set of Auger spectra recorded over $h\nu$ = 67.7–81.9 eV, no adjustments were made to the detector position or the timing circuit, so the energy-conversion parameters (the path length and the channel at which TOF = 0) were the same. Thus, the correspondence between channel number and energy was fixed. In Fig. 7 are plotted the same set of channel numbers for two spectra recorded at different photon energies; the TOF and kinetic energy scales apply to both spectra.

Niehaus has developed a semiclassical model which describes PCI effects on Auger decay for the case of inner-shell photoionization.[23] Near the ionization threshold, the photoelectron is still close enough to the ionic core, at the time of ejection of the Auger electron, to effectively modify the Coulomb field in which the Auger decay occurs. Energy exchanges occur between the "slow" photoelectron and the "fast" Auger electron. The Auger lines exhibit an asymmetric broadening, with the maxima of their energy distributions shifted to higher energy. The lines

in the present TOF spectra generally have asymmetric shapes anyway, due to the asymmetric shape of the source region of ejected electrons which are collected by the detectors.[31] However, the shifting and broadening effects are apparent in Fig. 7.

In the semiclassical model of Niehaus, the shift ε of the maximum in the energy distribution of the Auger line, relative to its position in the absence of PCI, is related to the core-hole lifetime τ and photoelectron energy E by the expression[67] (in atomic units)

$$\tau^{-1}[2(E + \varepsilon)]^{1/2} - \varepsilon(4E + 5\varepsilon) = 0. \tag{17}$$

Here, the "photoelectron energy" is a parameter (the "excess energy"), strictly defined as $E = h\nu - I$, where I is the ionization energy. The photoelectrons give up some energy to the Auger electrons. Also, Eq. (17) applies for negative values of E. In this model, the shift ε is determined only by the energy E and the decay width $\Gamma = \tau^{-1}$. The recent measurements of Schmidt et al.[22] of the shift ε for the Xe $N_5O_{2,3}O_{2,3}\ ^1S_0$ line fit well to the theoretical relation of Eq. (17) with a value $\Gamma = 110$ meV for the level width. This value for Γ agrees well with the widths of the $4d \rightarrow np$ resonances measured in the photoabsorption spectrum,[25] and not quite as well with those determined from electron energy-loss spectroscopy.[68]

From the TOF spectra, we measured the relative shift $\Delta\varepsilon$ of the $N_5O_1O_1\ ^1S_0$ peak with respect to its position at $h\nu = 81.9$ eV (note that with a width $\Gamma = 110$ meV, Eq. (17) predicts an absolute shift $\varepsilon =$

53 meV at $h\nu$ = 81.9 eV). Similar shifts were observed for the other N_5OO lines.

Schmidt and co-workers[69] first reported observations of the shifting and asymmetric broadening of Auger lines for the case of near-threshold inner-shell photoionization. They have recently reported a more extensive set of measurements and given a complete discussion of this particular type of PCI phenomenon and a detailed comparison of experiment with theory.[22] The main objective of our discussion has been to establish the presence of the PCI factor in our spectra. Nevertheless, Fig. 8 shows that the present measurements of the Auger line shift ε are in excellent agreement with the results of Schmidt et al.[22] and the theoretical relation Eq. (17) for a decay width Γ = 110 meV. Note that the present results plotted in Fig. 8 are the absolute values $\varepsilon = \Delta\varepsilon$ + 53 meV, i.e., corrected for the residual shift of 53 meV at our reference energy $h\nu$ = 81.9 eV. The results of Schmidt et al.[22] are relative shifts, however those authors took account of the variation of the theoretical Auger line energy distribution when convoluted with their spectrometer function. With this correction, the theoretical prediction for the relative shift which is appropriate to their data is essentially identical to the theoretical curve for the absolute shift over the energy range plotted in Fig. 8.

The areas of the Auger peaks in the 0° and 54.7° TOF spectra were obtained using a least-squares curve fitting routine, using asymmetric Gaussian functions with a linear background. The curves drawn through the spectra shown in Fig. 7 are examples of these fits. In the

deconvolution of lines 3-5 (see Fig. 5), a weak Auger line (number 26 in Ref. 47) between lines 4 and 5 was included. β values and intensity ratios were then determined for the lines numbered 1-7 in Fig. 5.

The β values for the three pairs of $N_{4,5}OO$ Auger lines are plotted in Fig. 9. The theoretical curve is that for a transition of the general type $N_5OO\ ^1S_0$, and was obtained using the Hartree-Fock (HF) calculations[10] of the partial-wave photoionization cross sections and Eqs. (2),(11), and (13). The β values based on the HF-length and the HF-velocity calculations differ by only 0.01-0.04 β units over the energy range of the experimental data. We have used the average of the length and velocity results for the theoretical curve in Fig. 9. In the presently adopted nonrelativistic model of the photoionization process, the same partial-wave branching ratio $\gamma(\varepsilon)$ (Eq. (2)) applies to both the N_5 and N_4 hole states at the same photoelectron energy ε. Thus, the alignment tensors $A_{20}(\varepsilon)$ for the $^2D_{5/2}$ and $^2D_{3/2}$ states differ by a constant factor determined by the two values for the constant C in Eq. (13). Taking account of this factor and the difference in the decay parameters α in Eq. (9), one finds that at a given photoelectron energy, $\beta(N_4OO\ ^1S_0) = (7/8)\beta(N_5OO\ ^1S_0)$. On a photon energy scale, however, the theoretical curve for an $N_4OO\ ^1S_0$ transition is shifted by 2 eV from that for an $N_5OO\ ^1S_0$ transition due to the N_5-N_4 spin-orbit splitting. As a result, the theoretical curve for $\beta(N_4OO\ ^1S_0)$ essentially overlaps the one plotted in Fig. 9 for $\beta(N_5OO\ ^1S_0)$, i.e., the two transitions should have nearly the same β at a given photon energy.

The results for the $N_{4,5}O_1O_1$ $^1S_0$ lines show that indeed the N_4- and N_5-OO $^1S_0$ lines have about the same β values at the same photon energy, and that the theoretical curve predicts the measured asymmetries well. The measurements also show that all of these Auger lines, independent of final state (including line number 4 (results not plotted)), have about the same β values; i.e., their Auger decay parameters α do not differ greatly. As predicted, the asymmetry parameters are relatively large near threshold where the $4d \rightarrow \varepsilon p$ photoionization channel dominates due to the centrifugal barrier for the f wave. The data follow the theoretical curve well from threshold as β steadily decreases, but drop below the curve near 76 eV. We were unable to explain this drop. Within the precision of the measurements, the overall agreement with theory is good. This conclusion holds even if the original assignment[47] of the $N_{4,5}O_1O_1$ $^1S_0$ lines is correct, since all of the low energy lines studied here have the same β values.

It can be seen from the theoretical expression Eq. (13) that the alignment tensor has a maximum value $A_{20}(\max) = Ca$ for $\gamma >> 1$ and a minimum value $A_{20}(\min) = C$ for $\gamma << 1$. Accordingly, the Auger electron asymmetry parameters also have limited ranges: $\alpha C \leq \beta \leq \alpha Ca$. For example, $0.229 \leq \beta(N_5OO\ ^1S_0) \leq 0.8$ and $0.2 \leq \beta(N_4OO\ ^1S_0) \leq 0.7$. Hence, A_{20} and β are not very sensitive to very large or very small values of γ, where asymptotic values are approached. The central 90% of the ranges of A_{20} and of β occur for γ values in the range $1/19 \leq \gamma \leq 19$.

Inverting Eq. (13) and using Eq. (9) gives an expression for γ as a function of β:

$$\gamma = \frac{\beta - \alpha C}{\alpha C a - \beta} \quad . \tag{18}$$

The γ values determined using the present set of β measurements for the $N_{4,5}O_1O_1\ ^1S_0$ lines are in qualitative agreement with the Hartree-Fock calculations, which follows considering the good agreement shown in Fig. 9. However, the uncertainties in our β measurements translate into very large uncertainties in γ, particularly for the very large and very small γ values, where β is less sensitive to the precise value of γ. A big improvement in the precision of the β measurements would be required, for example, to make a quantitative determination of the large values of γ produced near threshold or near the Cooper minimum.

The N_5OO:N_4OO Auger electron branching ratios were measured for the three pairs of $N_{4,5}OO$ lines identified in Table II. A few very weak Auger lines, which were not resolved in our spectra, occur near the $5s5p^5\ ^1P_1$ lines (see Ref. 47). These could cause small errors in the branching ratios for this final state. The measurements for the final states $5s^25p^3(^2P)5d\ ^1P_1$ and $5s^05p^6\ ^1S_0$ are plotted in Fig. 10 along with a theoretical curve[50] and measurements[51,52] for the $4d_{5/2}$:$4d_{3/2}$ photoelectron branching ratio. The Auger electron ratios agree well with the corresponding photoelectron ratios. The Auger measurements confirm indirectly that the $4d_{5/2}$:$4d_{3/2}$ ratio increases from threshold, as predicted, before decreasing at higher energy.

Somewhat larger values of the Auger branching ratio were measured near threshold for the $5s^05p^6\ ^1S_0$ final state than for the other two final states. The lower resolution set of TOF Auger spectra also gave a larger ratio near threshold for the $5s^05p^6\ ^1S_0$ lines than for the $5s5p^5\ ^1P_1$

lines. However, this distinction was not observed at higher energies where the ratios are smaller. This variation with final state of the $N_5OO:N_4OO$ ratio may be due simply to the kinetic energy dependence of the Coulomb matrix element. The 2 eV difference in the N_4OO and N_5OO energies is comparatively largest for the $5s^05p^6\ {}^1S_0$ lines, which occur at the lowest kinetic energies. Thus, the largest variation of the Coulomb transition strength would occur for those lines.

Also of interest are the intensity ratios for Auger decay to the various final states. Those ratios were determined for the four N_5OO transitions which were analyzed in our spectra (line numbers 2, 4, 5, and 7 in Fig. 5). In the spectra recorded at energies $h\nu \geq 69.7$ eV, the intensity ratios were constant to within 5%. Relative to line number 2, the measured intensity ratios for the line numbers 7:5:4:2 were 125:158:99:100. Except for the $5s^05p^6\ {}^1S_0$ final state (line number 7), the present results are in fairly good agreement with intensity ratios measured by Werme et al. using electron impact excitation; the ratios reported in Ref. 47 are 166:168:93:100. In the two spectra recorded nearest the N_5 threshold, there was an indication of a variation of the intensity ratios from the constant values measured at higher energies, which could conceivably arise as an effect of PCI. However, our limited data set precludes a definitive conclusion.

In discussing the results of the Auger electron measurements we have adopted the two-step model of the Auger process in which the formation of the inner-shell vacancy state and its decay are considered to be independent processes. This approximation appears to be valid at photon energies far enough above the 4d ionization threshold, but the effects of

PCI displayed in Figs. 7 and 8 demonstrate that the two-step model breaks down near threshold. In the near threshold region, the photoionization and Auger decay are more properly treated as a single process.[71,72] However, the present measurements of Auger electron angular distributions and branching ratios appear to be well described by the two-step model.

V. Autoionization of the 4d → np States

Photoabsorption spectra[24,25] of Xe recorded through the energy region $h\nu \approx 65$–70 eV display two Rydberg series of excitations which are described by the transitions

$$h\nu + Xe(4d^{10}5s^{2}5p^{6}\ {}^{1}S_{0}) \rightarrow Xe(4d^{9}5s^{2}5p^{6}({}^{2}D_{5/2,3/2})np\ {}^{1}P_{1}), \qquad (19)$$

where n = 6, 7, 8, ... These are the series of $4d_{5/2} \rightarrow np$ and $4d_{3/2} \rightarrow np$ resonant excitations which have as series limits the $(4d^{-1})\ {}^{2}D_{5/2}$ and ${}^{2}D_{3/2}$ ionic states. Because these "discrete" levels lie energetically above several lower ionization thresholds, they decay by autoionization into the accessible continuum channels. Fano has used the configuration-interaction formalism to describe the mixed discrete-continuum nature of an autoionizing state and to parameterize the resonance lineshape of the photoabsorption spectrum.[73] However, much more detailed information on the autoionization process is obtained by using electron spectroscopy to observe resonance effects on the individual final states. The magnitudes and phases of the photoionization amplitudes can vary rapidly through a resonance, resulting in resonance structure in the photoelectron cross sections, angular distributions, and spin-polarization parameters.[74–76] Starace has extended Fano's theory to describe partial photoionization cross sections and photoelectron branching ratios within an isolated resonance.[75] Similarly, Kabachnik and Sazhina have formulated the resonance behavior of the photoelectron

angular distribution and spin polarization.[76] In the general case, however, there are several overlapping Rydberg series, which interact. A unified and comprehensive description of autoionization in this general case is obtained using the multichannel quantum defect theory (MQDT).[77] For the entire resonance region, the MQDT generates resonance profiles for all of the dynamical parameters which can be observed using electron spectroscopy, i.e., partial photoionization cross sections and the photoelectron asymmetry and spin-polarization parameters (for example, see Ref. 78).

A. Resonant Auger Ionization

In the present experiment, the Xe 4d $\rightarrow$ np resonances were located by recording photoelectron excitation spectra such as the one shown in Fig. 11. Photoelectrons from both the 0° and 54.7° TOF detectors were collected in this spectrum as the monochromator was stepped through the resonance region. The spectrum was recorded at a fixed sample gas density, but is uncorrected for variation of the photon beam intensity, which increased by about 50% from $h\nu$ = 63 eV to 72 eV. A "window" was placed on the time-to-amplitude converter of the detector circuit so that only the resonantly produced Auger electrons[26,27] were counted, i.e., the 5p and 5s photoelectrons were excluded. It was found that the resonance structure in the excitation spectrum was much less distinct when the 5p and 5s photoelectrons were included. Since the Auger electrons are produced only as a result of 4d excitation, they are highly sensitive to the resonance structure in the photoabsorption spectrum.

In Fig. 11 and following figures we use the notation $4d^{-1}(^2D_{5/2})$ or $4d^{-1}(^2D_{3/2})$ to represent a vacancy in the 4d subshell. The resonance line positions and ionization thresholds reported by Codling and Madden[24] are indicated in Fig. 11. The shapes and intensities of the resonance features in Fig. 11 are in accord with the high resolution photoabsorption spectrum.[25] The strongest excitations, $4d_{5/2} \rightarrow 6p$ and $4d_{3/2} \rightarrow 6p$, stand out, and smaller features also appear, due to the $4d \rightarrow 7p$ transitions. Excitation spectra served both to calibrate the energy scale of the monochromator and to determine the photon bandpass. The spectrum in Fig. 11 was recorded with the smallest bandpass used in these experiments, 1.2 Å FWHM (0.4 eV at $h\nu = 65$ eV). Our bandpass was considerably larger than the natural widths ($\Gamma \simeq 0.1$ eV) of the resonances.[25] The energy calibration of the monochromator appears to be accurate to within ±0.1 eV in the energy region of the resonances, based on the reproducibility of the observed position of the $4d^{-1}(^2D_{5/2})6p$ peak in several excitation spectra.

Several final states could be populated by the decay of the $4d \rightarrow np$ resonances. Consider the following possible decay channels following $4d \rightarrow 6p$ photoexcitation:

$$Xe(4d^9 5s^2 5p^6 (^2D)6p\ ^1P_1) \rightarrow Xe^+(4d^{10} 5s^2 5p^5\ ^2P) + e^- \quad (20)$$

$$\rightarrow Xe^+(4d^{10} 5s5p^6\ ^2S) + e^- \quad (21)$$

$$\rightarrow Xe^+(4d^{10} 5s^2 5p^4 (^1D)5d\ ^2S) + e^- \quad (22)$$

$$\rightarrow Xe^+(4d^{10} 5s^2 5p^4 (^1S)6p\ ^2P) + e^- \quad (23)$$

$$\rightarrow Xe^+(4d^{10} 5s5p^5 (^1P)6p\ ^2L) + e^- \quad (24)$$

$$\rightarrow Xe^+(4d^{10} 5s^0 5p^6 (^1S)6p\ ^2P) + e^- \quad (25)$$

In all of these decay processes at least two electrons change quantum numbers: one fills the 4d vacancy and another is ejected. Processes (20) and (21) are the usual "autoionization" transitions: the 6p Rydberg electron changes quantum numbers, and the final states are the primary "one-electron" ionic states, which are also produced off resonance by direct ionization. Transition (22) represents a (formally) more complicated combination of autoionization and final ionic state configuration interaction (FISCI), which was discussed earlier. The final state of Eq. (22) represents a FISCI satellite of the 5s photoline[62] and is also produced off resonance. The transitions of Eqs. (23)-(25) are "Auger" processes and differ qualitatively from those of Eqs. (20)-(22). The 6p electron remains in the final state while one O-shell electron fills the 4d vacancy and another is ejected. The final states are the same as those formed by $N_{4,5}OO$ Auger decay above the ionization threshold, but with a 6p "spectator" electron remaining. These resonant Auger final states are not observed to be produced off resonance by direct ionization (very small off-resonance intensities are indicated theoretically[64]). Note that the resonant Auger states described by the configurations $5s^2 5p^4(SL)np$ occur in the same energy region as the 5s-FISCI satellites,[62] but that the two sets of states are distinguished by having opposite parities.

In Fig. 12 are shown 54.7° TOF spectra of Xe recorded at photon energies both on and off resonance, with a bandpass of 1.7 Å FWHM (0.6 eV at $h\nu$ = 65 eV). The spectra have been scaled in the figure to

account for variations in the photon beam intensity, sample gas density, and collection time. The relative transmission of the detector was approximately constant over the range of electron energies recorded in the spectra. Hence, the areas of the peaks as they appear in the figure are proportional to the partial photoionization cross sections. The first spectrum in Fig. 12 was recorded at $h\nu$ = 63.4 eV, which is below the resonance region, so only direct ionization occurs. The photolines produced are the 5p, 5s, and 5s satellites. The 5s satellites[60] have been assigned[62] to configurations of the type $5s^2 5p^4(SL)nd$ and $5s^2 5p^4(SL)ns$. The spectrum recorded at $h\nu$ = 65 eV, i.e., at the $4d^{-1}(^2D_{5/2})6p$ resonance, is highly modified from the off-resonance spectrum. The series of lines labeled $5s^2 5p^4 n\ell$ are strongly enhanced, and a set of lower energy lines, with considerable intensities, also appear. These results are attributed to the Auger decay of the resonant state. The enhanced intensity of the lines labeled $5s^2 5p^4 n\ell$ is due to the Auger final states $5s^2 5p^4(SLJ)6p$, rather than the 5s satellites which occur in the same energy region. In addition, higher resolution electron spectra recorded at this resonance by Eberhardt et al.[27] and others[22,26] show that these Auger lines are accompanied by strong shake-up transitions to the levels $5s^2 5p^4(SLJ)7p$. The spectrum recorded at $h\nu$ = 65.8 eV is again off resonance, and only the direct ionization final states are observed. In the 67 eV spectrum, recorded at the $4d^{-1}(^2D_{3/2})6p$ resonance, the Auger final states are again produced.

The resonant Auger spectra in Fig. 12 have the same general appearance as the Auger spectrum recorded above the 4d ionization threshold. However, in the resonant spectra only one line appears for each final state, while two lines per final state are produced above threshold due to transitions from both of the N_5 and N_4 vacancy states. The lower energy Auger lines numbered 1-4 in Fig. 12 correspond to the lines in Fig. 5 which were studied above threshold. We assign the resonant Auger lines accordingly, by appending a 6p spectator electron. The assignments are listed in Table III along with binding energies determined by energy conversion of the TOF spectra. Line number 2 in Fig. 12 appears to correspond to line number 4 in Fig. 5, which we have left unassigned. The spectrum in Fig. 12 recorded at the $4d^{-1}(^2D_{5/2})6p$ resonance ($h\nu$ = 65 eV) corresponds well with the spectrum shown in Ref. 26, where the lines $5s5p^5 6p$ and $5s^0 5p^6 6p$ are identified as they are here. The binding energies listed in Table III agree well with those obtained from the spectrum in Ref. 26. Re-analysis of certain energy levels of Xe II led Hansen and Persson[28] to propose a revised identification of the resonant Auger spectrum of Xe recorded by Eberhardt et al.[27] From the revised analysis it was determined that the effect of the 6p spectator electron is to shift the kinetic energies of the resonant Auger lines $5s^2 5p^4(SLJ)6p$ to about 4.4 eV higher than observed above threshold for the $5s^2 5p^4(SLJ)$ multiplets. Similarly, with the assignments given in Table III, we measure kinetic energy shifts of between 4.1-4.9 eV for the lower energy Auger lines in comparison with their energies in the absence of a 6p spectator electron.

The resonant Auger lines 2 and 3 in Fig. 12 correspond to the satellite Auger lines observed above threshold and discussed earlier. It is interesting to notice that lines 2 and 3 alternate intensities between the two strong resonances $4d^{-1}(^2D_{5/2})6p$ and $4d^{-1}(^2D_{3/2})6p$. This observation was reproduced in another set of spectra.

The asymmetry parameter for the resonant Auger line $5s5p^5(^1P_1)6p$ was $\beta = 0.85 \pm 0.15$ in the two spectra recorded at 65 eV and 67 eV. This value agrees with those measured for the N_5OO Auger lines at the $4d^{-1}(^2D_{5/2})$ threshold.

If the intensity scales of the resonant Auger spectra are expanded to bring out weak features, peaks are observed over the kinetic energy region $\epsilon \simeq 8$–19 eV (energies $\epsilon < 8$ eV were not recorded in the spectra). The energies and intensities of these weak lines indicate that they arise from autoionization of the resonant Auger states identified in Table III to the levels $5s^25p^4(SLJ)$ of Xe III.

It is clear from the spectra in Fig. 12 that the intensities of the 5p and 5s photolines are relatively unaffected by the $4d \rightarrow 6p$ resonant excitation but that the Auger final states are strongly populated. These qualitative features of the spectra are further displayed in Fig. 13 where relative partial cross sections are plotted. The cross sections for 5p and 5s photoelectrons stay relatively constant through the resonance region, while the transitions to the $5s^25p^4n\ell$ lines are resonantly enhanced. Off resonance, the $5s^25p^4n\ell$ lines are identified to be the 5s satellites. We measured an off-resonance branching ratio of about 1:1 for the sum of the intensities

of the 5s satellites to the intensity of the 5s line. This is in agreement with the relative intensities measured using X-ray photoelectron spectroscopy[60] and the FISCI calculation of Hansen and Persson.[62] The higher resolution electron spectra of Refs. 22, 26, and 27 show that the enhanced intensity of the $5s^2 5p^4 n\ell$ transitions at the 4d → 6p resonances is due to the Auger final states rather than the 5s satellites. The intensities of the 5s satellites appear to remain relatively unaffected by autoionization, like the 5s main line.

The effects of the Auger decay process on resonant photoemission have been studied theoretically.[72,73,79,80] Though, essentially, it is not the case here with Xe 4d photoexcitation, it would be of considerable interest to observe resonant Auger transitions which are produced simultaneously by a nonresonant ionization process. In such a case, an asymmetric Fano-type intensity profile would, in general, result due to interference between the resonant and nonresonant transition amplitudes. In the absence of an interference effect, the resonant Auger decay results in a symmetric Lorentzian profile in the partial cross section. In the present case the total photoabsorption cross section could display asymmetric profiles at the resonances due to interference structure in the 5p, 5s, and 5s-satellite channels. However, the high resolution photoabsorption spectrum of Ederer and Manalis[25] shows essentially symmetrical Lorentzian lineshapes and with nearly constant linewidths (however, see also Ref. 68). These observations indicate that the resonances decay primarily by the Auger process which is free of an interference effect and that the 5p, 5s,

and 5s-satellite decay channels are relatively weak. These expectations are confirmed by the electron spectra in Fig. 12 and the partial cross sections in Fig. 13. It is not surprising that the 4d → np resonances decay preferentially by the Auger process, since the Coulomb interaction e/r_{ij} between a pair of O-shell electrons is stronger than that between an O-shell electron and the np Rydberg electron.

B. 5p and 5s Resonant Photoemission

Although the partial photoionization cross section for the 5p subshell showed little variation upon resonant excitation, the asymmetry parameter β increased at the resonant energies. This effect was observed from spectra such as in Fig. 12 where the spin-orbit split $5p_{3/2}$ and $5p_{1/2}$ photoelectrons were unresolved. The recent measurements of Codling et al. and of Ederer et al.,[81] for example, made in the region of the Xe $5s5p^6 6p\ ^1P_1$ resonance have shown variations between the resonance profiles of $\beta(5p_{3/2})$ and $\beta(5p_{1/2})$ and an oscillation in the $5p_{3/2}:5p_{1/2}$ branching ratio. Theoretical work has shown that resonant variations of partial cross sections, branching ratios, and photoelectron asymmetry and spin-polarization parameters are expected as a general phenomenon.[74-76] These observable parameters characterize the interaction of the resonant states with the continuum channels. Hence, we recorded a series of 0° and 54.7° TOF spectra of the resolved 5p doublet through the energy region of the 4d → np resonances.

An example from the TOF spectra of the 5p doublet is shown in Fig. 14. In the resonance region, the 5p photoelectrons are produced with about 50 eV kinetic energy. The TOF detectors are equipped with simple retarding-grid units which comprise about 60% of the total flight path. A 35 V retarding potential was applied to resolve the 5p doublet. A bandpass of 1.2 Å FWHM (0.4 eV at $h\nu$ = 65 eV) was used in recording spectra in the resonance region. Collection times of about 4000 sec were required to collect 1000-4000 counts in each peak. To obtain peak areas for determining partial cross sections, branching ratios, and asymmetry parameters, the spectra were fitted to the form of asymmetric Gaussian functions with a linear background.

The results for the partial cross sections, branching ratio, and asymmetry parameters are plotted in Figs. 15 and 16. Also plotted in Fig. 16 are previous measurements of the asymmetry parameters[18] and the branching ratio.[18,82] Since the present set of spectra were recorded with a monochromator bandpass (0.4 eV FWHM) which is considerably larger than the widths of the resonant states (~0.1 eV),[25] any resonance structure in the photoelectron dynamical parameters might be reduced by averaging with the nonresonant background. A small oscillation in the $5p_{3/2}$ cross section was observed near the most intense resonant state, $4d^{-1}(^2D_{5/2})6p$. Very little structure is apparent in the $5p_{1/2}$ cross section measurements. However, distinct resonance structure was observed in both β parameters. Maxima in the β values occur near the strong $4d \rightarrow 6p$ excitations, and smaller features appear at the 7p resonances. Also, the measurement at

$h\nu = 67.7$ eV indicates that the β values increase in the energy gap just above the $4d_{5/2}$ ionization threshold and below the $4d_{3/2} \rightarrow 7p$ resonance. This feature is similar to the sustained rise of the β parameters above the $4d_{3/2}$ threshold (see Fig. 2 and Ref. 18). A distinct oscillation in the $5p_{3/2}$:$5p_{1/2}$ branching ratio was observed near the $4d_{5/2} \rightarrow 6p$ excitation. Krause et al.[18] also measured a dip in the branching ratio near this first strong resonance. Additional structure in the branching ratio at the higher energy resonances is not apparent, perhaps due in part to cancellation of overlapping structures.

The $4d^{-1}(^2D_{5/2})6p$ excitation is the strongest among the members of the two series and is well separated from the higher energy resonances. The Auger spectrum resulting from the decay of this resonant state has been studied here and previously.[22,26,27] In the present set of measurements, this resonance produced the only distinct structure in the partial cross sections and branching ratio of the 5p doublet and the most pronounced structure in the asymmetry parameters. Hence, the $4d_{5/2} \rightarrow 6p$ resonance seems to offer a good example for theoretical studies of inner-shell photoexcitation and autoionization.

Cheng and Johnson have used the relativistic random-phase approximation (RRPA) to calculate partial photoionization cross sections, photoelectron asymmetry parameters, and spin-polarization parameters for the Xe $5p_{3/2}$, $5p_{1/2}$, and 5s subshells in the energy region of the $4d_{5/2}$ 6p resonance.[29] The Auger decay channels were not included in their calculations. In Fig. 17 we compare the present measurements of $\beta(5p_{3/2})$ and $\beta(5p_{1/2})$ with the RRPA theory. Also shown are curves obtained by fitting the data to the theoretical functional form for the resonance profile of β through an isolated resonance.[76] To account for the monochromator bandpass, the fitting functions were convoluted with a triangular function having 0.4 eV FWHM. The fitted curves obtained after deconvolution of the bandpass function are also plotted in Fig. 17. The experimental results confirm that $\beta(5p_{1/2}) > \beta(5p_{3/2})$ as predicted, but note that the experimental β profiles show considerably bigger resonance widths than theory, even after deconvolution of the bandpass.

The discrepancy in the widths is apparently due to the absence of the Auger decay channels in the theoretical calculation. Only the $5p_{3/2}$, $5p_{1/2}$, and 5s decay channels were included in the RRPA calculation, and the calculated widths of the resonance features in the partial cross sections are on the order of 0.01 eV. These are much smaller than the observed resonance width (~0.1 eV), which is determined primarily by the Auger decay. However, the calculated widths of the resonance features in the β parameters are ~0.1 eV, much larger than the calculated widths for the cross sections. Similarly, deconvolution of the bandpass from the experimental results gives a β profile with a larger width (~0.2 eV) than

that observed in the photoabsorption spectrum. This probably explains in part why more distinct structure was experimentally observed in the β parameters than in the cross sections; i.e., averaging over the monochromator bandpass had a more severe effect in the case of the cross sections than for the β parameters. However, an additional factor here, which is also related to the widths of the resonance features, is that the β parameter includes interference terms which depend on the phases of the photoionization amplitudes as well as the magnitudes. Thus, as noted by Dill,[74] the resonance in β can be more pronounced than in the cross section.

The final set of results are measurements of the angular distribution of Xe 5s photoelectrons through the region of the 4d → np resonances and just above the 4d ionization threshold. The photoionization process is

$$h\nu + Xe(5s^2 5p^6\ {}^1S_0) \rightarrow Xe^+(5s5p^6\ {}^2S_{1/2}) + e^-(\varepsilon p) \quad . \tag{26}$$

Dehmer and Dill have shown that the analysis of this process is clarified by use of the angular momentum transfer formulation.[83] Angular momentum and parity conservation restrict the photoelectron to a p wave. In a nonrelativistic model the spins of the photoelectron and ionic core remain coupled into a singlet, and an energy-independent asymmetry parameter $\beta = 2$ is predicted. However, the spin-orbit interaction provides a mechanism for reorienting the spins into a triplet. The triplet channel is characterized by an energy-independent

asymmetry parameter $\beta = -1$, and the observed asymmetry is a weighted average of the singlet and triplet contributions:

$$\beta_{5s}(\varepsilon) = \frac{2\sigma_S(\varepsilon) - \sigma_T(\varepsilon)}{\sigma_S(\varepsilon) + \sigma_T(\varepsilon)} \quad , \qquad (27)$$

where $\sigma_S(\varepsilon)$ and $\sigma_T(\varepsilon)$ are the energy-dependent cross sections for production of singlet and triplet final states, respectively. Thus, values over the entire range $-1 \leq \beta_{5s}(\varepsilon) \leq 2$ are possible, and the observed value can be interpreted as a measure of the relative strengths for production of singlet and triplet final states.

Strong deviations of $\beta(5s)$ from the nonrelativistic value 2 have been measured at photon energies near the Cooper minimum.[17,83] A quantitative interpretation of this result is given by the RRPA calculations which include interchannel coupling with the 5p and 4d subshells.[84] The transition strength of the singlet channel passes through a minimum near $h\nu \simeq 35$ eV, so that the triplet contribution becomes relatively stronger. The observable result is that $\beta(5s)$ oscillates through a minimum.

The present measurements of $\beta(5s)$ are plotted in Fig. 18. The measurements were made in an energy region far from the Cooper minimum, and large asymmetries were observed. This result is in good agreement with the RRPA[14,37] and Dirac-Fock (DF)[85] theories, as well as other calculations[86] not plotted in Fig. 18. Torop et al.[16] also

measured $1.8 < \beta(5s) \leq 2$ at $h\nu = 83$ eV. Values in the range $\beta(5s) = 1.8$–2.0 indicate a contribution from the triplet channel of less than 7% of the total transition strength.

The RRPA calculation of $\beta(5s)$ plotted in Fig. 18 includes interchannel coupling with the 5p and 4d subshells, but the effects of autoionizing $4d \rightarrow np$ resonances were smoothed over in the results shown. As discussed above, additional RRPA calculations have been made to study the effects of the $4d^{-1}(^2D_{5/2})6p$ excitation on 5p and 5s photoionization.[29] As for the $5p_{3/2}$ and $5p_{1/2}$ subshells, a strong resonant enhancement in the 5s partial cross section is calculated. From an off resonance value of $\beta(5s) \approx 2$, the calculation obtains a resonant feature $\beta(5s) \rightarrow -1$, indicating that the triplet channel of 5s photoionization couples strongly with the resonant state. However, no indication of this effect is apparent in the measured $\beta(5s)$ values. The measurements in the resonance region were obtained with a 1.7 Å FWHM bandpass (0.6 eV at $h\nu = 65$ eV), so any resonance structure might be considerably reduced by the nonresonant contribution. It seems, though, that such a strong oscillation, which extends over the entire range of the β parameter, would still have been detected. We suggest that the amplitude of any resonance structure is much less than calculated, because the Auger channels dominate the decay of the resonance.

The RRPA calculations, in combination with the multichannel quantum-defect theory, are highly successful in calculating the resonance profiles of photoelectron dynamical parameters for the case of the

Beutler-Fano autoionizing resonances of the rare gases.[78] The present case of inner-shell photoexcitation differs from the outer-shell cases in that the resonances decay primarily into the Auger final states.[87] The present measurements of cross sections and β parameters for 5p and 5s photoelectrons indicate the importance of including the Auger decay channels in theoretical calculations of inner-shell autoionization.

VI. Conclusions

Several aspects of inner-shell photoexcitation and ionization of Xe were investigated in these experiments. The present results for the 5p $\beta(\varepsilon)$ parameter extend those of previous measurements which confirm that the (4d,5p) interchannel coupling completely modifies the angular distribution of 5p photoelectrons, particularly above the 4d ionization threshold.

We observed the broadening and shifting of N_5OO Auger electron peaks due to post-collision interaction near the 4d ionization threshold, in good agreement with previous measurements and theory. The $N_{4,5}OO$ Auger electrons are produced with anisotropic angular distributions due to alignment of Xe^+ $(4d^{-1})$ by photoionization. The measured β values of $N_{4,5}OO$ Auger electrons are in good agreement with theoretical calculations. The alignment and corresponding Auger electron asymmetries are relatively large near the 4d ionization threshold as a consequence of the centrifugal barrier in the $4d \rightarrow \varepsilon f$ channel.

As expected, the $4d^{-1}(^2D_{5/2,3/2})np$ resonances were observed to decay primarily by the Auger process. Relatively little structure was observed in the 5p and 5s photoionization cross sections, but distinct structure was produced in the angular distributions of $5p_{3/2}$ and $5p_{1/2}$ photoelectrons. For the 5s photoelectrons we measured $\beta \simeq 2$, with no indication of a resonance effect. Comparison of the measurements with theoretical calculations for autoionization of the $4d^{-1}(^2D_{5/2})6p$ resonance indicates the need to include the Auger decay channels in the calculations. However, the measurements were obtained using a monochomator

bandpass which is rather large compared with the decay widths of the resonances. In order to compare theory with experiment quantitatively, it is desirable to measure the resonance structure with a smaller bandpass.

Acknowledgments

We thank B. Pate for his work in aligning the beam line optics and monochromator. We are grateful to S. T. Manson, W. R. Johnson, and K. T. Cheng for helpful discussions and for providing their unpublished theoretical results.

This work was supported by the Director, Office of Energy Research, Office of Basic Energy Sciences, Chemical Sciences Division of the U.S. Department of Energy under Contract No. DE-AC03-76SF00098. It was performed at the Stanford Synchrotron Radiation Laboratory, which is supported by the NSF through the Division of Materials Research. One of us (U.B.) acknowledges the support of the Deutsche Forschungsgemeinschaft.

References

1. S. H. Southworth P. H. Kobrin, C. M. Truesdale, D. W. Lindle, S. Owaki, and D. A. Shirley, Phys. Rev. A 24, 2257 (1981).
2. V. L. Jacobs, J. Phys. B 5, 2257 (1972).
3. C. N. Yang, Phys. Rev. 74, 764 (1948).
4. H. K. Tseng, R. H. Pratt, S. Yu, and A. Ron, Phys. Rev. A 17, 1061 (1978).
5. D. L. Ederer, Phys. Rev. Lett. 13, 760 (1964).
6. A. P. Lukirskii, I. A. Brytov, and T. M. Zimkina, Opt. Spektrosk. 17, 438 (1964) (translation: Opt. Spectrosc. 17, 234 (1964)); A. P. Lukirskii, I. A. Brytov, and S. A. Gribovskii, Opt. Spektrosk. 19, 368 (1965) (translation: Opt. Spectrosc. 20, 203 (1966)).
7. R. Haensel, G. Keitel, P. Schreiber, and C. Kunz, Phys. Rev. 188, 1375 (1969).
8. J. W. Cooper, Phys. Rev. Lett. 13, 762 (1964).
9. S. T. Manson and J. W. Cooper, Phys. Rev. 165, 126 (1968).
10. D. J. Kennedy and S. T. Manson, Phys. Rev. A 5, 227 (1972).
11. M. Ya. Amusia and N. A. Cherepkov, Case Stud. Atom. Phys. 5, 47 (1975).
12. M. Ya. Amusia and V. K. Ivanov, Phys. Lett. A 59, 194 (1976).
13. M. Ya. Amusia, Comments Atom. Mol. Phys. 8, 61 (1979).
14. W. R. Johnson and K. T. Cheng, Phys. Rev. A 20, 978 (1979).
15. J. B. West, P. R. Woodruff, K. Codling, and R. G. Houlgate, J. Phys. B 9, 407 (1976); M. Y. Adam, F. Wuilleumier, N. Sandner, S. Krummacher, V. Schmidt, and W. Mehlhorn, Jap. J. Appl. Phys. 17-2, 170 (1978).

16. L. Torop, J. Morton, and J. B. West, J. Phys. B 9, 2035 (1976).

17. M. G. White, S. H. Southworth, P. Kobrin, E. D. Poliakoff, R. A. Rosenberg, and D. A. Shirley, Phys. Rev. Lett. 43, 1661 (1979) and 44, 620(E) (1980).

18. M. O. Krause, T. A. Carlson, and P. R. Woodruff, Phys. Rev. A 24, 1374 (1981).

19. A. F. Starace, Appl. Opt. 19, 4051 (1980).

20. S. Flügge, W. Mehlhorn, and V. Schmidt, Phys. Rev. Lett. 29, 7 (1972).

21. E. G. Berezhko, N. M. Kabachnik, and V. S. Rostovsky, J. Phys. B 11, 1749 (1978).

22. V. Schmidt, S. Krummacher, F. Wuilleumier, and P. Dhez, Phys. Rev. A 24, 1803 (1981).

23. A. Niehaus, J. Phys. B 10, 1845 (1977).

24. K. Codling and R. P. Madden, Phys. Rev. Lett. 12, 106 (1964).

25. D. L. Ederer and M. Manalis, J. Opt. Soc. Am. 65, 634 (1975).

26. V. Schmidt, Appl. Opt. 19, 4080 (1980). Fig. 10 of this reference shows a photoelectron spectrum of Xe recorded at the $4d^9 5s^2 5p^6 (^2D_{5/2}) 6p\ ^1P_1$ resonance, obtained from N. Sandner, Ph.D. Thesis, Universität Freiburg (1978) and other unpublished work.

27. W. Eberhardt, G. Kalkoffen, and C. Kunz, Phys. Rev. Lett. 41, 156 (1978). A revised identification of the resonant Auger spectrum of Xe recorded by Eberhardt et al. has been given in Ref. 28.

28. J. E. Hansen and W. Persson, Phys. Rev. A 20, 364 (1979).

29. K. T. Cheng and W. R. Johnson (unpublished).

30. F. C. Brown, R. Z. Bachrach, and N. Lien, Nucl. Instrum. Meth. 152, 73 (1978).

31. M. G. White, R. A. Rosenberg, G. Gabor, E. D. Poliakoff, G. Thornton, S. H. Southworth, and D. A. Shirley, Rev. Sci. Instrum. 50, 1268 (1979).

32. R. F. Davis, S. D. Kevan, B.-C. Lu, J. G. Tobin, and D. A. Shirley, Chem. Phys. Lett. 71, 448 (1980).

33. S. Southworth, C. M. Truesdale, P. H. Kobrin, D. W. Lindle, W. D. Brewer, and D. A. Shirley, J. Chem. Phys. 76, 143 (1982).

34. F. Wuilleumier and M. O. Krause, J. Electron Spectrosc. 15, 15 (1979).

35. J. L. Dehmer, W. A. Chupka, J. Berkowitz, and W. T. Jivery, Phys. Rev. A 12, 1966 (1975).

36. The $\beta(5p)$ values from Refs. 18 and 35 which are plotted in Fig. 2 are weighted averages of $\beta(5p_{3/2})$ and $\beta(5p_{1/2})$, with weights given by the experimental $5p_{3/2}:5p_{1/2}$ branching ratio reported in Ref. 18.

37. K.-N. Huang, W. R. Johnson, and K. T. Cheng, At. Data Nucl. Data Tables 26, 33 (1981) and unpublished results.

38. W. Ong and S. T. Manson, Phys. Rev. A 21, 842 (1980).

39. B. Cleff and W. Mehlhorn, Phys. Lett. A 37, 3 (1971); J. Phys. B 7, 605 (1974).

40. U. Fano, Rev. Mod. Phys. 29, 74 (1957).

41. U. Fano, Phys. Rev. 90, 577 (1953).

42. A. J. Ferguson, Angular Correlation Methods in Gamma-Ray Spectroscopy (Wiley, New York, 1965).

43. K. Blum and H. Kleinpoppen, Phys. Reports 52, 203 (1979).

44. B. Cleff and W. Mehlhorn, J. Phys. B 7, 593 (1974).

45. E. G. Berezhko and N. M. Kabachnik, J. Phys. B 10, 2467 (1977).

46. The expressions for α given in Ref. 45 are for the case where angles are measured with respect to the propagation direction of the photon beam rather than the polarization direction. In order that the factor α in Eq. (9) be consistent with the general definition of an asymmetry parameter β (Eq. (1)), it is necessary to multiply the α values of Ref. 45 by -2.

47. L. O. Werme, T. Bergmark, and K. Siegbahn, Phys. Scr. 6, 141 (1972). According to the analysis of Hansen and Persson (Ref. 28), the kinetic energies of the Xe $N_{4,5}OO$ Auger lines reported by Werme et al. should be increased by 0.2 eV to agree with the measurements of Ref. 48.

48. S. Ohtani, H. Nishimura, H. Suzuki, and K. Wakiya, Phys. Rev. Lett. 36, 863 (1976).

49. E. G. Berezhko, V. K. Ivanov, and N. M. Kabachnik, Phys. Lett. A 66, 474 (1978).

50. W. R. Johnson and V. Radojević, J. Phys. B 11, L773 (1978). We have shifted the theoretical curve to lower photon energy by 4.1 eV to coincide with the experimental ionization threshold rather than the theoretical threshold.

51. S. P. Shannon, K. Codling, and J. B. West, J. Phys. B 10, 825 (1977).

52. M. Y. Adam, F. Wuilleumier, S. Krummacher, N. Sandner, V. Schmidt, and W. Mehlhorn, J. Electron Spectrosc. 15, 211 (1979).

53. M. S. Banna, M. O. Krause, and F. Wuilleumier, J. Phys. B 12, L125 (1979).

54. J. B. West, P. R. Woodruff, K. Codling, and R. G. Houlgate, J. Phys. B 9, 407 (1976); J. B. West and J. Morton, At. Data Nucl. Data Tables 22, 103 (1978).

55. C. E. Moore, Atomic Energy Levels, Natl. Bur. Stand. (U.S.) Circ. No. 467 (U.S. GPO, Washington, D.C., 1958), Vol. III.

56. W. Mehlhorn, W. Schmitz, and D. Stalherm, Z. Phys. 252, 399 (1972).

57. F. P. Larkins, J. Phys. B 6, 2450 (1973); E. J. McGuire, Phys. Rev. A 11, 17 (1975).

58. F. P. Larkins, At. Data Nucl. Data Tables 20, 311 (1977) and 23, 587(E) (1979).

59. H. Hertz, Z. Phys. A 274, 289 (1975).

60. U. Gelius, J. Electron Spectrosc. 5, 985 (1974).

61. M. Y. Adam, F. Wuilleumier, N. Sandner, V. Schmidt, and G. Wendin, J. Phys. (Paris) 39, 129 (1978).

62. J. E. Hansen and W. Persson, Phys. Rev. A 18, 1459 (1978).

63. G. Wendin, Phys. Scr. 16, 296 (1977).

64. K. G. Dyall and F. P. Larkins, J. Phys. B 15, 203 and 219 (1982).

65. S. T. Manson, J. Electron Spectrosc. 9, 21 (1976); D. A. Shirley, J. Phys. (Paris) 39, C4-35 (1978).

66. Excitations of the type $np^2 \rightarrow n'd^2$ have been shown to be significant in describing photoionization of the outer np subshells

of the rare gases. See J. R. Swanson and L. Armstrong, Jr., Phys. Rev. A 15, 661 (1977) and 16, 1117 (1977); also, Ref. 19 and references therein.

67. Note that there is a typographical error in Eq. (16) of Ref. 23; a factor of 4 should multiply the δ in the second term.

68. G. C. King, M. Tronc, F. H. Read, and R. C. Bradford, J. Phys. B 10, 2479 (1977).

69. V. Schmidt, N. Sandner, W. Mehlhorn, M. Y. Adam, and F. Wuilleumier, Phys. Rev. Lett. 38, 63 (1977).

70. V. Schmidt, N. Sandner, W. Mehlhorn, F. Wuilleumier, and M. Y. Adam, in Proceedings of the Tenth International Conference on the Physics of Electronic and Atomic Collisions, Paris, 1977 (North-Holland, Amsterdam, 1978), p. 1062.

71. M. Ya. Amusia, Appl. Opt. 19, 4042 (1980) and references therein; T. Åberg, Phys. Scr. 21, 495 (1980).

72. G. Wendin, in Photoionization of Atoms and Molecules, Proceedings of the Daresbury Meeting, edited by B. D. Buckley, Report No. DL/SCI/R11 (1978), p. 1; in Proceedings of the Sixth International Conference on VUV Radiation Physics, Charlottesville, 1980, extended abstracts II-87.

73. U. Fano, Phys. Rev. 124, 1866 (1961); U. Fano and J. W. Cooper, ibid. 137, A1364 (1965); Rev. Mod. Phys. 40, 441 (1968).

74. D. Dill, Phys. Rev. A 7, 1976 (1973).

75. A.F. Starace, Phys. Rev. A 16, 231 (1977).

76. N.M. Kabachnik and I.P. Sazhina, J. Phys. B 9, 1681 (1976).

77. For surveys of the MQDT see U. Fano, J. Opt. Soc. Am. 65, 979 (1975); A. F. Starace, in Photoionization and Other Probes of Many-Electron Interactions, edited by F. J. Wuilleumier (Plenum, New York, 1976), p. 395.

78. W. R. Johnson, K. T. Cheng, K.-N. Huang, and M. Le Dourneuf, Phys. Rev. A 22, 989 (1980).

79. F. H. Mies, Phys. Rev. 175, 164 (1968).

80. Y. Yafet, Phys. Rev. B 21, 5023 (1980) and 23, 3558 (1981); L. C. Davis and L. A. Feldkamp, Phys. Rev. B 23, 6239 (1981); F. Combet Farnoux, Phys. Rev. A 25, 287 (1982).

81. K. Codling, J. B. West, A. C. Parr, J. L. Dehmer, and R. L. Stockbauer, J. Phys. B 13, L693 (1980); D. L. Ederer, A. C. Parr, J. B. West, D. Holland, and J. L. Dehmer, Phys. Rev. A 25, 2006 (1982).

82. F. Wuilleumier, M. Y. Adam, P. Dhez, N. Sandner, V. Schmidt, and W. Mehlhorn, Phys. Rev. A 16, 646 (1977).

83. J. L. Dehmer and D. Dill, Phys. Rev. Lett. 37, 1049 (1976).

84. W. R. Johnson and K. T. Cheng, Phys. Rev. Lett. 40, 1167 (1978).

85. W. Ong and S. T. Manson, J. Phys. B 11, L65 (1978); Phys. Rev. A 19, 688 (1979).

86. T. E. H. Walker and J. T. Waber, J. Phys. B 7, 674 (1974); N. A. Cherepkov, Phys. Lett. A 66, 204 (1978); K.-N. Huang and A. F. Starace, Phys. Rev. A 21, 697 (1980).

87. The present measurements indicate that the resonances decay by $\gtrsim$ 90% into the Auger channels.

Table I. Hartree-Fock calculations of Kennedy and Manson[10] for the partial-wave branching ratio γ (Eq. (2)) for photoionization of the Xe 4d subshell as a function of photoelectron energy ε. Also listed are the resulting theoretical values (Eqs. (11) and (13)) for the alignment tensor A_{20} of Xe^+ $^2D_{5/2}$ and the asymmetry parameter β for an Auger transition of the type N_5OO $^1S_0$. Results are given for both the length and velocity forms of the dipole operator.

	HF-L			HF-V		
ε(Ry)	γ	A_{20}	β	γ	A_{20}	β
0.00	1.467+1	0.357	0.764	1.843+1	0.360	0.771
0.05	7.769	0.344	0.735	9.806	0.349	0.747
0.10	4.677	0.327	0.699	5.927	0.336	0.718
0.20	2.083	0.288	0.615	2.665	0.301	0.644
0.40	6.352-1	0.211	0.451	8.241-1	0.228	0.487
0.60	2.665-1	0.163	0.349	3.508-1	0.176	0.377
0.80	1.406-1	0.140	0.299	1.873-1	0.149	0.319
1.00	8.940-2	0.129	0.275	1.203-1	0.136	0.290
1.25	6.128-2	0.122	0.262	8.348-2	0.128	0.273
1.50	4.768-2	0.119	0.255	6.575-2	0.123	0.264
1.75	3.962-2	0.117	0.250	5.525-2	0.121	0.258
2.00	3.412-2	0.116	0.247	4.812-2	0.119	0.255
2.50	2.725-2	0.114	0.244	3.933-2	0.117	0.250
3.00	2.401-2	0.113	0.242	3.556-2	0.116	0.248
3.50	2.359-2	0.113	0.242	3.599-2	0.116	0.248
4.00	2.563-2	0.114	0.243	4.053-2	0.117	0.251
6.00	7.205-2	0.125	0.267	1.454-1	0.141	0.301
8.00	4.312-1	0.187	0.401	2.071	0.287	0.614
10.00	5.081+1	0.369	0.789	3.972	0.320	0.685
15.00	3.331-1	0.174	0.371	2.263-1	0.156	0.334
20.00	1.390-1	0.140	0.298	1.176-1	0.135	0.289
25.00	9.279-2	0.130	0.277	8.406-2	0.128	0.273
30.00	7.241-2	0.125	0.267	6.829-2	0.124	0.265

Table II. Identification of the Xe $N_{4,5}OO$ Auger lines indicated in Fig. 5. The kinetic energies are those reported by Werme et al., but increased by 0.2 eV due to a correction in calibration data (see Ref. 47). For comparison, the kinetic energies given by energy-conversion of the present TOF spectrum are also listed.

Line no.	Initial vacancy	Final state	Kinetic energy (eV) Werme et al.	TOF
1	N_4	$5s5p^5\ ^1P_1$	21.64 (5)	21.76 (5)
2	N_5	$5s5p^5\ ^1P_1$	19.65 (3)	19.72 (5)
3	N_4	$5s^25p^3(^2P)5d\ ^1P_1$	16.12 (5)	16.12 (5)
4	N_5	. . .	15.25 (6)	15.17 (5)
5	N_5	$5s^25p^3(^2P)5d\ ^1P_1$	14.15 (7)	14.09 (5)
6	N_4	$5s^05p^6\ ^1S_0$	10.27 (7)	10.22 (5)
7	N_5	$5s^05p^6\ ^1S_0$	8.28 (7)	8.24 (5)

Table III. Identification of the resonant Auger lines of Xe indicated in Fig. 12.

Line number	Final state	Binding energy (eV)
1	$5s5p^5(^1P_1)6p$	40.9 (2)
2	...	45.8 (3)
3	$5s^25p^3(^2P)5d(^1P_1)6p$	46.1 (3)
4	$5s^05p^6(^1S_0)6p$	52.1 (2)

Figure Captions

Fig. 1. Calibration function $f_0(\varepsilon)$ (Eq. (3)) used for determining asymmetry parameters $\beta(\varepsilon)$. Also shown is the $\beta(\varepsilon)$ parameter for Ne 2p photoelectrons,[34] which was used to obtain the calibration data points.

Fig. 2. Experimental and theoretical values of the Xe 5p photoelectron asymmetry parameter. Measurements: ●, Ref. 35; □, Ref. 18; Δ, Ref. 16; ○, present results (see Ref. 36). Theory (Ref. 12): random-phase approximation with exchange (RPAE) calculations which include (full curve) and do not include (dashed curve) interchannel coupling with the 4d subshell.

Fig. 3. Auger electron asymmetry parameters for the transitions Xe $N_5O_1O_1$ $^1S_0$ (open circles) and $N_5O_1O_{2,3}$ $^1P_1$ (closed circles). The theoretical curves (see text for references) are for a transition of the general type N_5OO $^1S_0$. Dashed curve: Hartree-Fock length; full curve: Hartree-Fock velocity. The energy of the preceding $4d_{5/2}$ photoelectron is also shown.

Fig. 4. Xe N_5OO:N_4OO Auger electron branching ratio compared with the $4d_{5/2}$:$4d_{3/2}$ photoelectron branching ratio. ●, Average of the Auger electron branching ratios $N_5O_1O_1$:$N_4O_1O_1$ ($^1S_0$) and $N_5O_1O_{2,3}$:$N_4O_1O_{2,3}$ ($^1P_1$). Experimental data for the $4d_{5/2}$:$4d_{3/2}$ photoelectron branching ratio: Δ, Ref. 51; ○, Ref. 52; □, Ref. 53. The theoretical curve is from the RRPA calculation, Ref. 50.

Fig. 5. Time-of-flight spectra of Xe $N_{4,5}OO$ Auger electrons produced following photoionization, at 0° and 54.7° relative to the polarization direction. A nonlinear energy scale is also given. The numbered lines are identified in Table II.

Fig. 6. The 54.7° time-of-flight spectrum of Xe Auger electrons recorded at a photon energy in between the $4d_{5/2}$ and $4d_{3/2}$ ionization thresholds. Only the N_5OO Auger lines were produced. The numbered peaks are identified in Table II.

Fig. 7. The Xe $N_5O_1O_1$ $^1S_0$ Auger line recorded at photon energies which lie 0.1 eV above the $4d_{5/2}$ ionization threshold (top) and at 14.4 eV above threshold (bottom). The shifting and broadening of the Auger line recorded near the ionization threshold are attributed to post-collision interaction.

Fig. 8. The energy shift of the Xe N_5OO Auger lines as a function of the $4d_{5/2}$ excess energy. The theoretical curve is that derived in Ref. 23 for an N_5-hole decay width of 110 meV. The curve is appropriate for both the absolute shifts ε plotted using the present measurements and for the relative shifts $\Delta\varepsilon$ of Ref. 22 which are corrected for the spectrometer function (see discussion in text). ●, Present measurements for the $N_5O_1O_1$ $^1S_0$ line. Measurements for the $N_5O_{2,3}O_{2,3}$ $^1S_0$ line: ○, Ref. 22; △, Ref. 69; □, Ref. 70.

Fig. 9. Asymmetry parameters for Xe $N_{4,5}OO$ Auger electrons. Each panel gives measurements for both the N_5 (closed circles) and N_4 (open circles) transitions which have the given final state. The same theoretical curve, based on Hartree-Fock calculations (see text for references), is plotted in all three panels, but is appropriate for transitions of the general type $N_{4,5}OO\ ^1S_0$. The two arrows mark the positions of the N_5 and N_4 ionization thresholds.

Fig. 10. Xe N_5OO:N_4OO Auger electron branching ratios compared with the $4d_{5/2}$:$4d_{3/2}$ photoelectron branching ratio. Present measurements of the Auger electron ratios: ●, $5s^05p^6\ ^1S_0$; ▲, $5s^25p^3(^2P)5d\ ^1P_1$. Measurements of the photoelectron ratio: ○, Ref. 52; □, Ref. 51. The theoretical curve (Ref. 50) is the RRPA calculation for the photoelectron branching ratio. The arrow marks the position of the N_4 ionization threshold.

Fig. 11. Photoelectron excitation spectrum of Xe recorded through the 4d → np resonances (see text for discussion). The positions of the resonances and the ionization thresholds are those reported by Codling and Madden.[24]

Fig. 12. Time-of-flight electron spectra of Xe recorded off resonance (at $h\nu$ = 63.4 eV and 65.8 eV) and at the resonances $4d^{-1}(^2D_{5/2})6p$ (65.0 eV) and $4d^{-1}(^2D_{3/2})6p$ (67.0 eV). The peaks numbered 1-4 are identified in Table III. A nonlinear kinetic energy scale is also given.

Fig. 13. Relative partial photoionization cross sections for Xe 5p (squares) and 5s (closed circles) photoelectrons and for the group of electron peaks in Fig. 12 labeled $5s^2 5p^4 n\ell$ (open circles). A line is drawn through the open circles to accent the resonant enhancement as suggested by the excitation spectrum in Fig. 11. The positions of the 4d → 6p resonances are indicated.

Fig. 14. 0° and 54.7° time-of-flight photoelectron spectra of the Xe 5p doublet recorded at $h\nu$ = 65.1 eV.

Fig. 15. Relative partial photoionization cross sections for the Xe $5p_{3/2}$ and $5p_{1/2}$ subshells measured in the energy region of the 4d → np resonances.

Fig. 16. Asymmetry parameters for Xe $5p_{3/2}$ and $5p_{1/2}$ photoelectrons and the $5p_{3/2}$:$5p_{1/2}$ branching ratio measured through the $4d^{-1}(^2D_{5/2,3/2})np$ resonances. Asymmetry parameters for $5p_{1/2}$ and $5p_{3/2}$ are denoted with open and closed symbols, respectively: circles, this work; squares, Ref. 18. Branching ratio: circles, this work; squares, Ref. 18; triangles, Ref. 82. Lines have been drawn through the data to indicate the resonance structure.

Fig. 17. Comparison of experiment and theory for the asymmetry parameters of Xe $5p_{3/2}$ and $5p_{1/2}$ photoelectrons produced at the $4d^{-1}(^2D_{5/2})6p$ resonance. The solid curves are the RRPA theoretical calculations (Ref. 29). The dashed curves are fits of the experimental data to the theoretical functional form derived in Ref. 76 for the resonance profiles, including convolution with the monochromator bandpass (0.4 eV FWHM). The dot-dashed curves are the fitted resonance profiles after deconvolution of the bandpass.

Fig. 18. Asymmetry parameter of Xe 5s photoelectrons compared with the DF (Ref. 85) and RRPA (Refs. 14 and 37) theoretical curves. Only a representative error bar is shown. The positions of the $4d^{-1}(^2D_{5/2,3/2})np$ resonances are indicated.

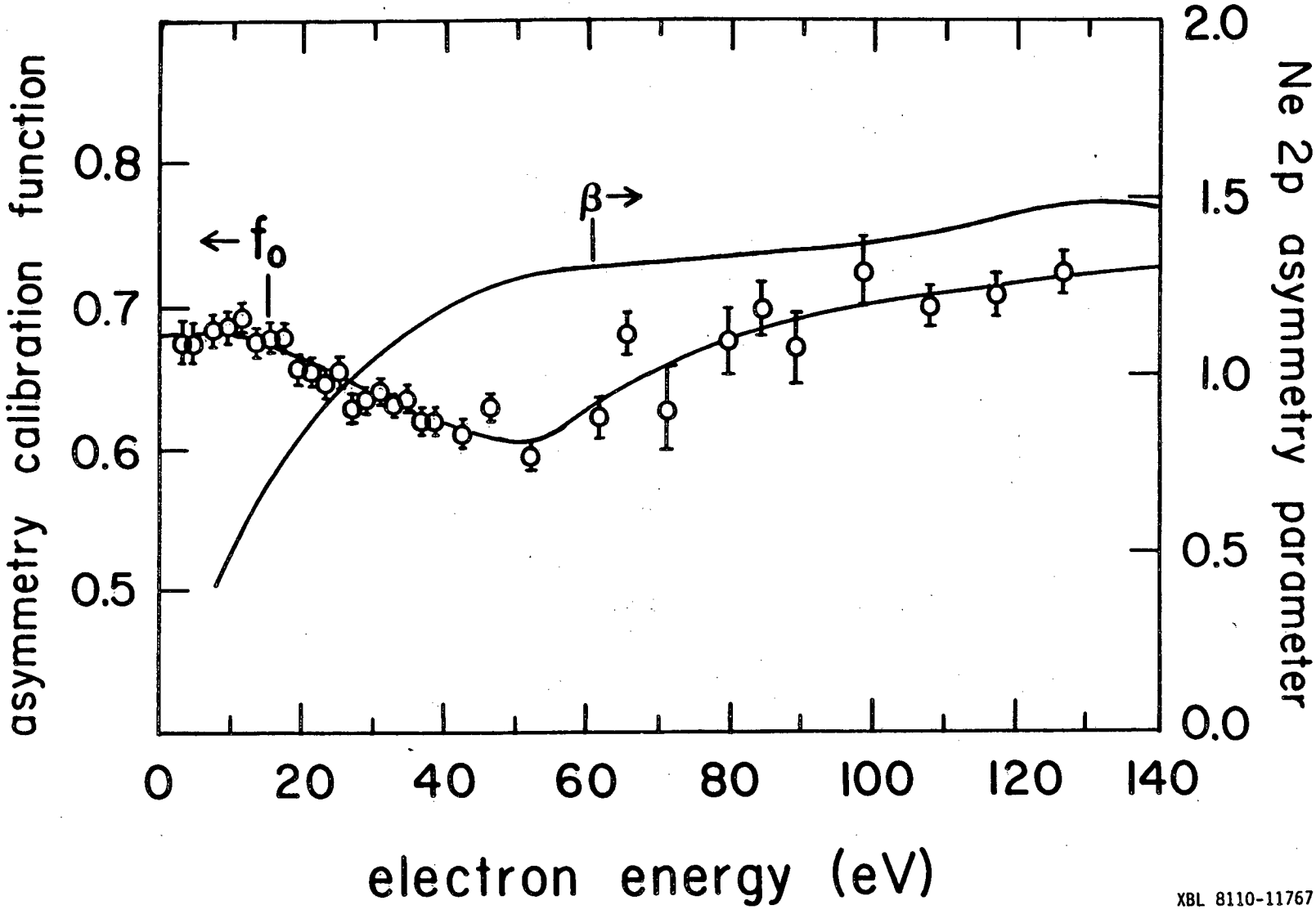

XBL 8110-11767

Figure 1

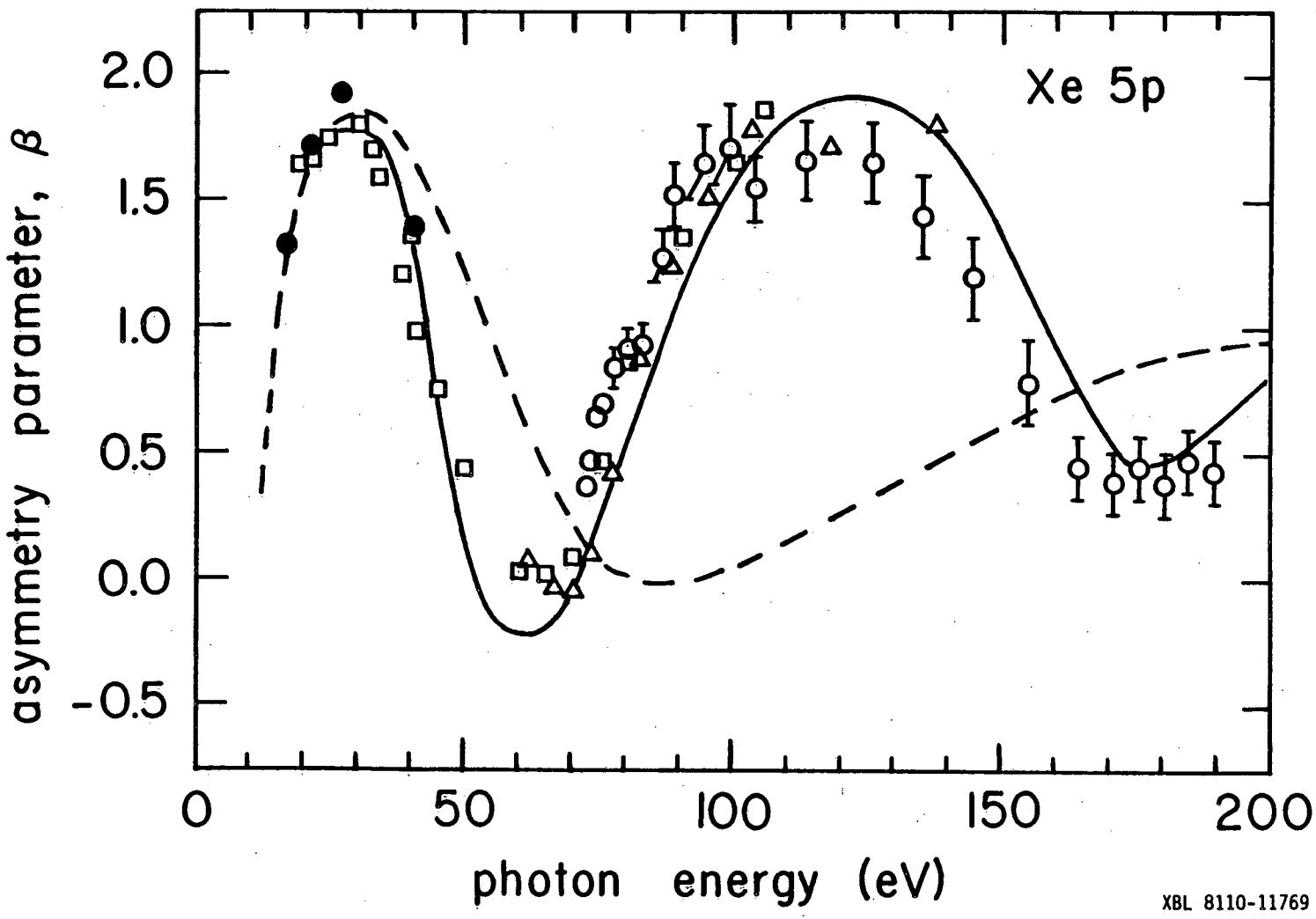

XBL 8110-11769

Figure 2

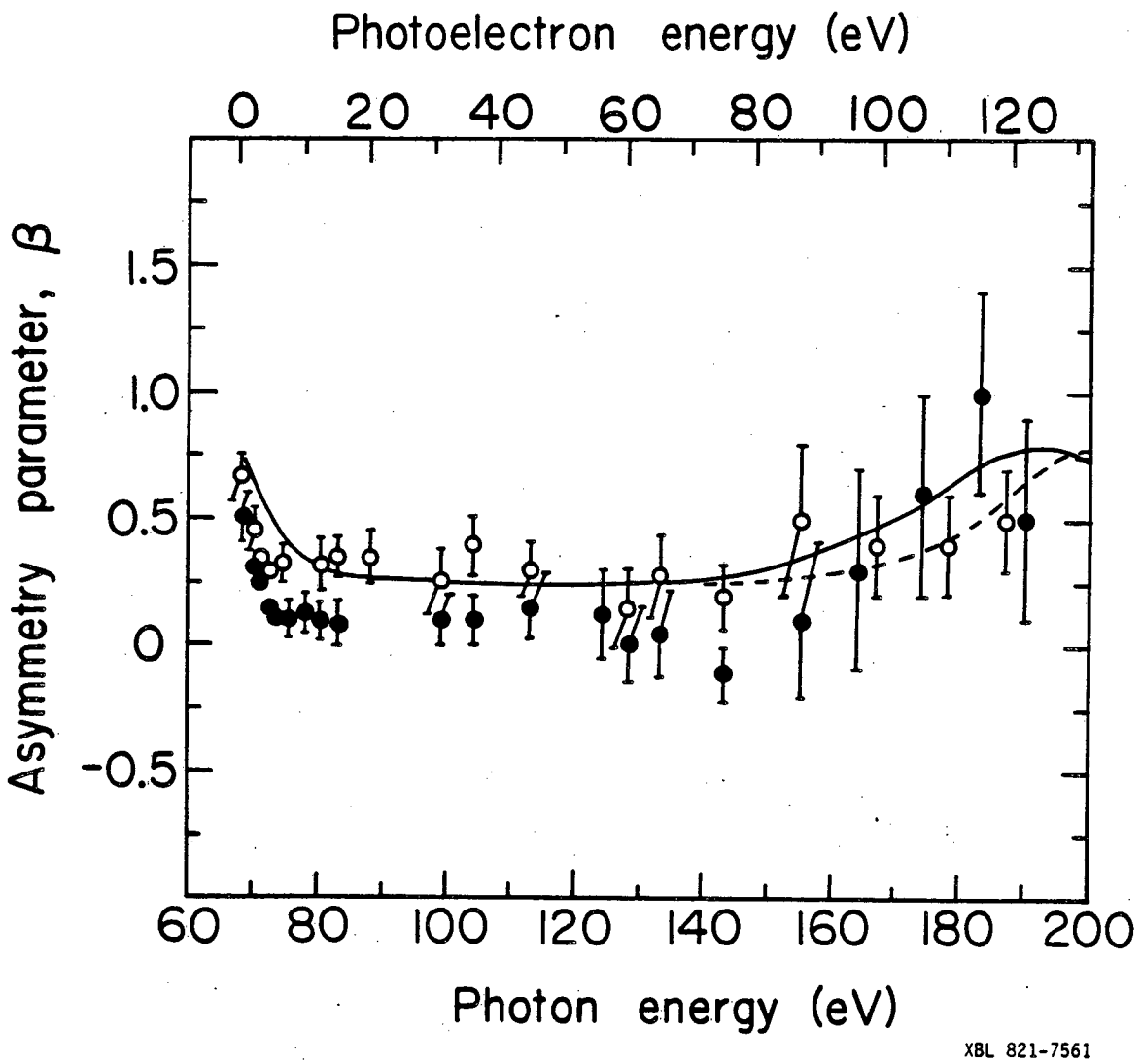
Photoelectron energy (eV)
0
20
40
60
80
100
120
Asymmetry parameter, β
1.5
1.0
0.5
0
-0.5
60
80
100
120
140
160
180
200
Photon energy (eV)
XBL 821-7561

Figure 3

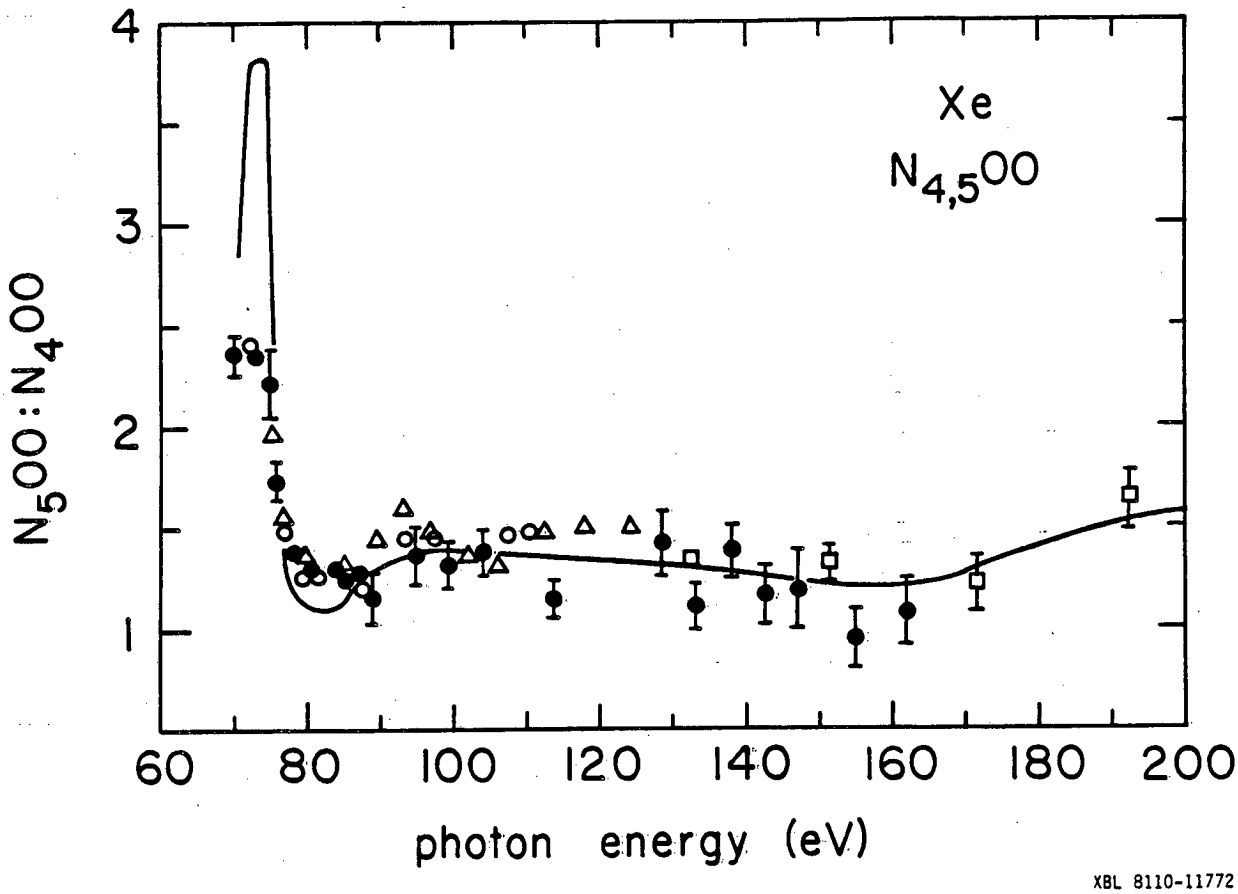
Xe
$N_{4,5}OO$
$N_5OO : N_4OO$
4
3
2
1
60
80
100
120
140
160
180
200
photon energy (eV)
XBL 8110-11772

Figure 4

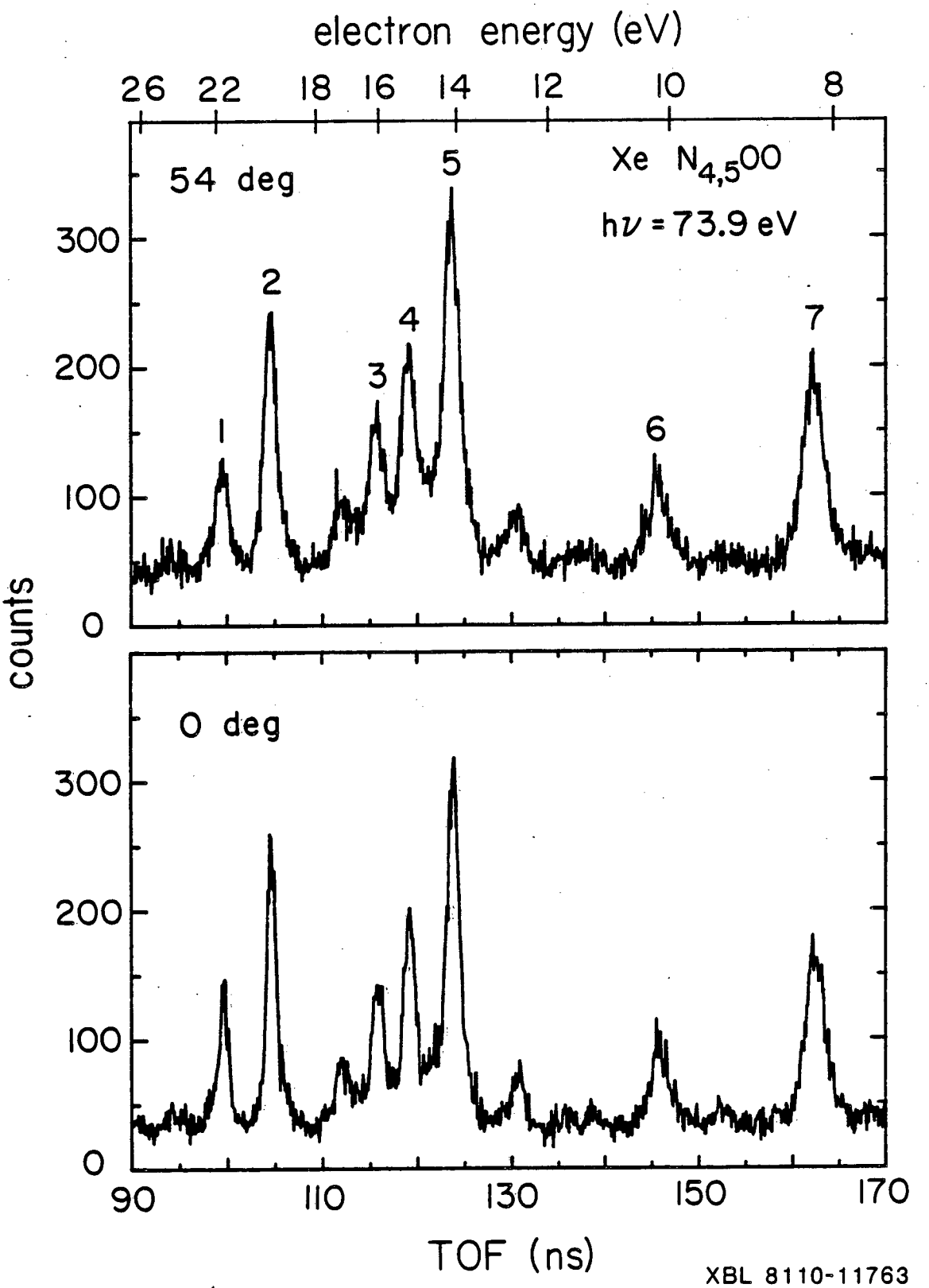
electron energy (eV)
26
22
18
16
14
12
10
8
54 deg
Xe $N_{4,5}OO$
$h\nu = 73.9$ eV
1
2
3
4
5
6
7
0 deg
counts
300
200
100
0
90
110
130
150
170
TOF (ns)
XBL 8110-11763

Figure 5

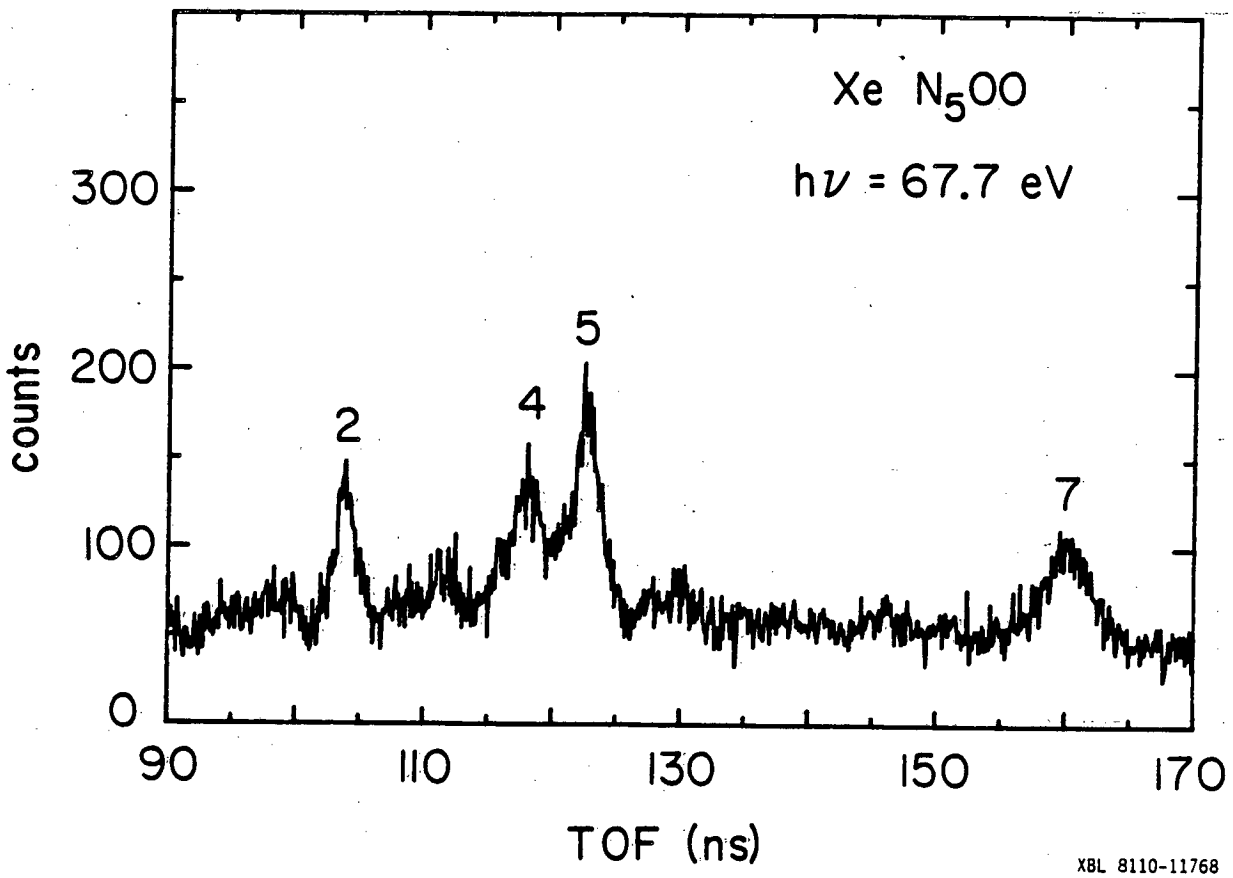
Xe N5OO
hν = 67.7 eV
counts
300
200
100
0
2
4
5
7
90
110
130
150
170
TOF (ns)
XBL 8110-11768

Figure 6

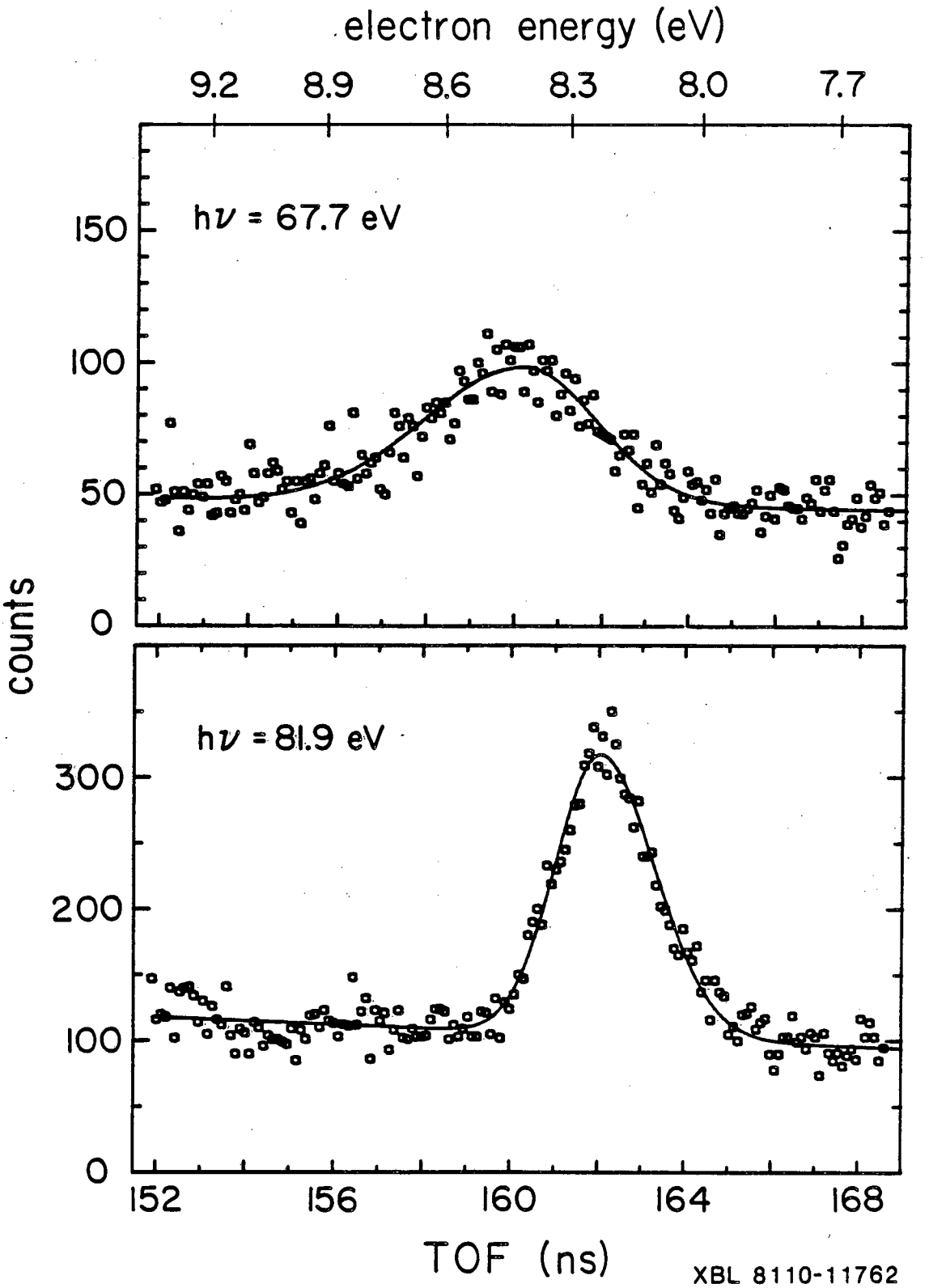
electron energy (eV)
9.2
8.9
8.6
8.3
8.0
7.7
hν = 67.7 eV
150
100
50
0
counts
hν = 81.9 eV
300
200
100
0
152
156
160
164
168
TOF (ns)
XBL 8110-11762

Figure 7

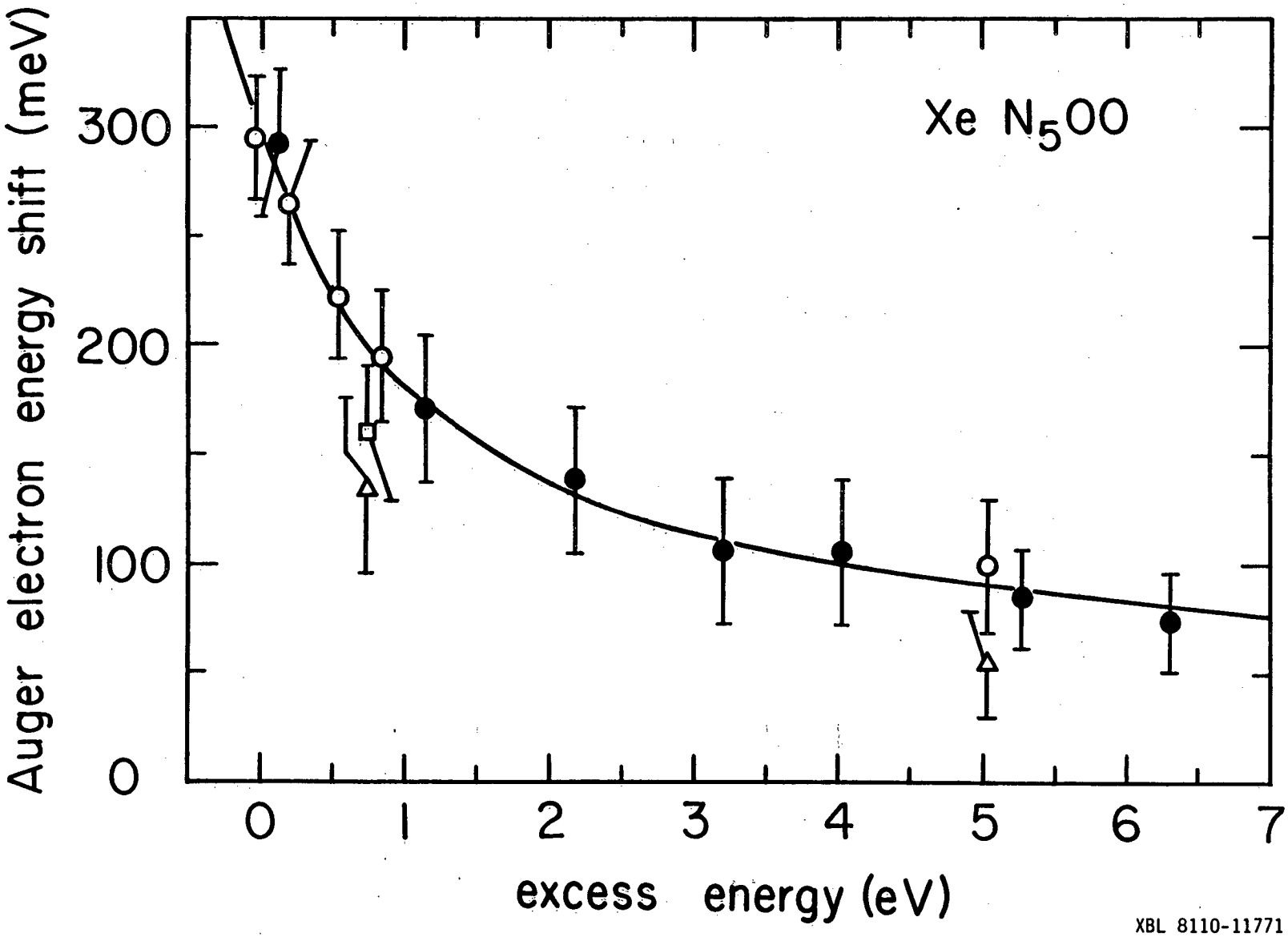

XBL 8110-11771

Figure 8

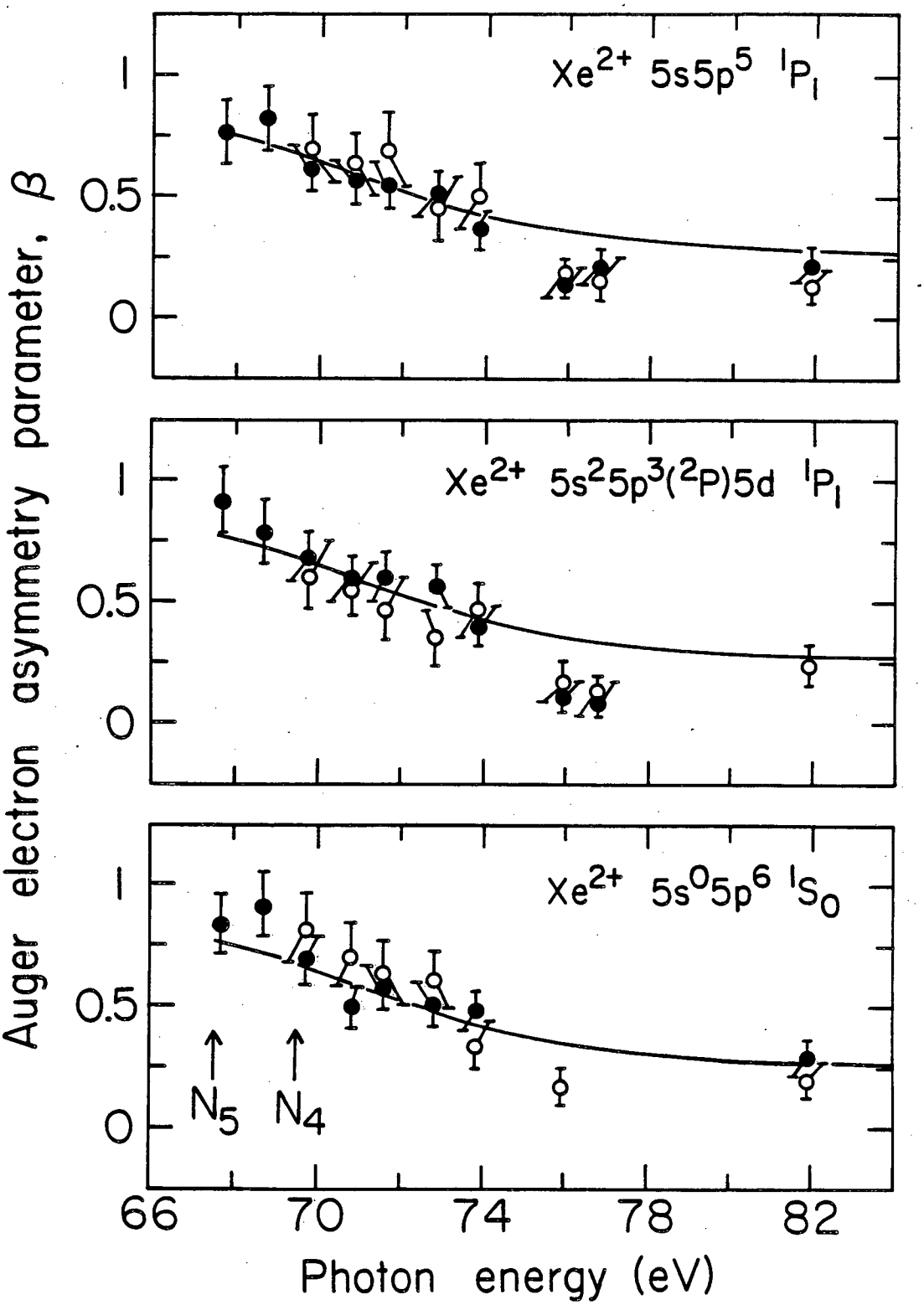

XBL 8112-13001

Figure 9

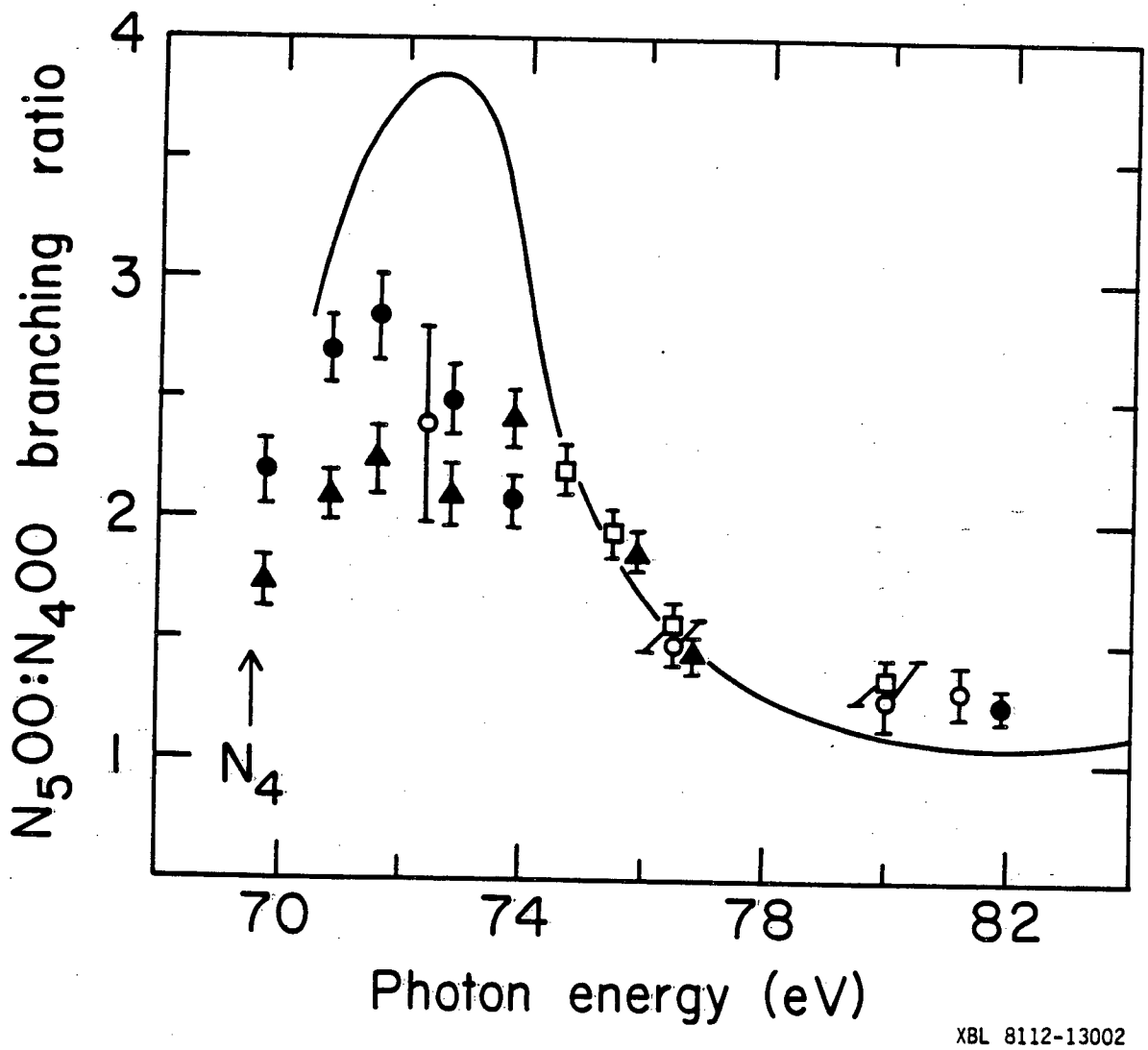
4
3
2
1
$N_5OO:N_4OO$ branching ratio
N_4
70
74
78
82
Photon energy (eV)
XBL 8112-13002

Figure 10

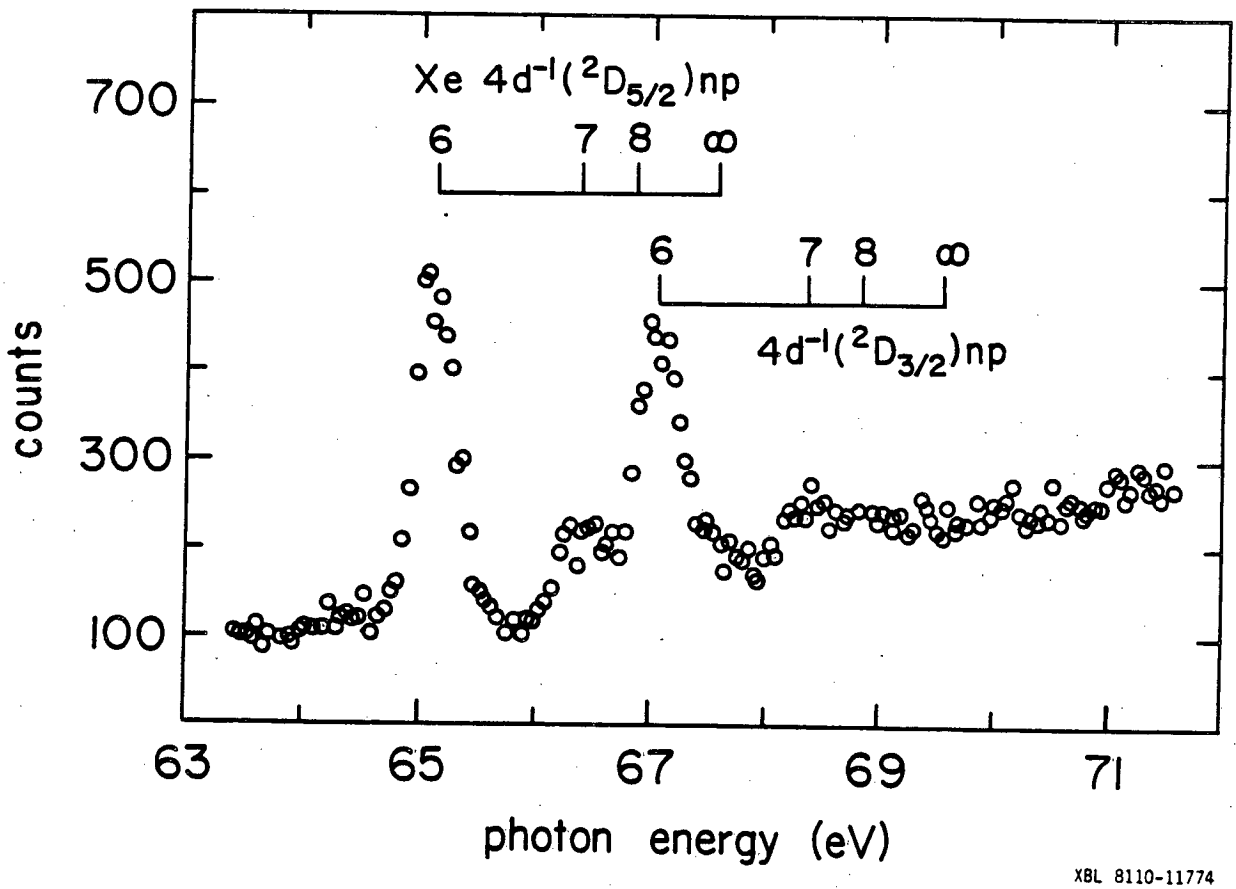
Xe 4d⁻¹(²D5/2)np
6
7
8
∞
6
7
8
∞
4d⁻¹(²D3/2)np
700
500
300
100
counts
63
65
67
69
71
photon energy (eV)
XBL 8110-11774

Figure 11

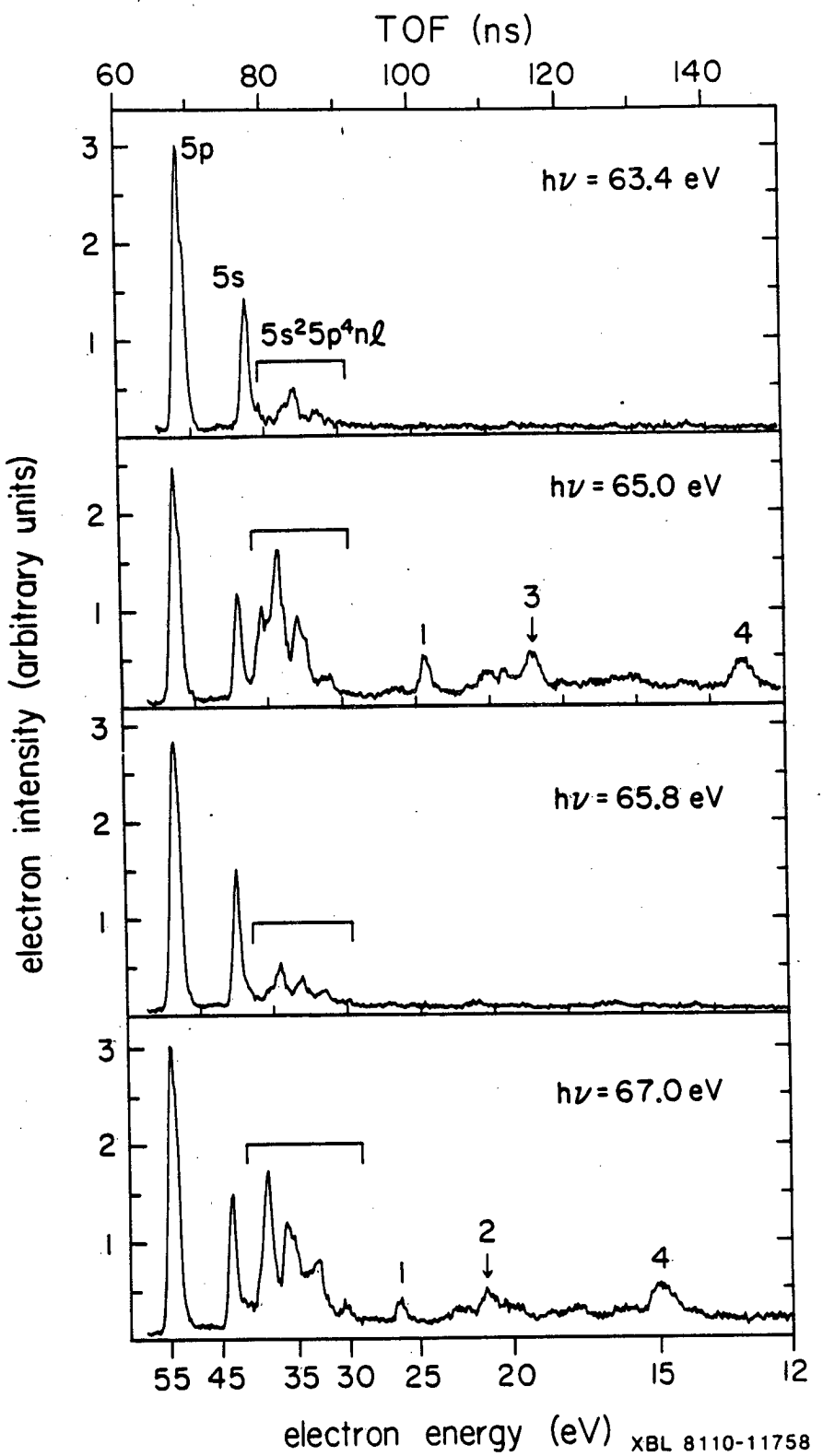
TOF (ns)
60
80
100
120
140
5p
5s
$5s^2 5p^4 n\ell$
hν = 63.4 eV
hν = 65.0 eV
hν = 65.8 eV
hν = 67.0 eV
1
2
3
4
electron intensity (arbitrary units)
55 45 35 30 25 20 15 12
electron energy (eV)
XBL 8110-11758

Figure 12

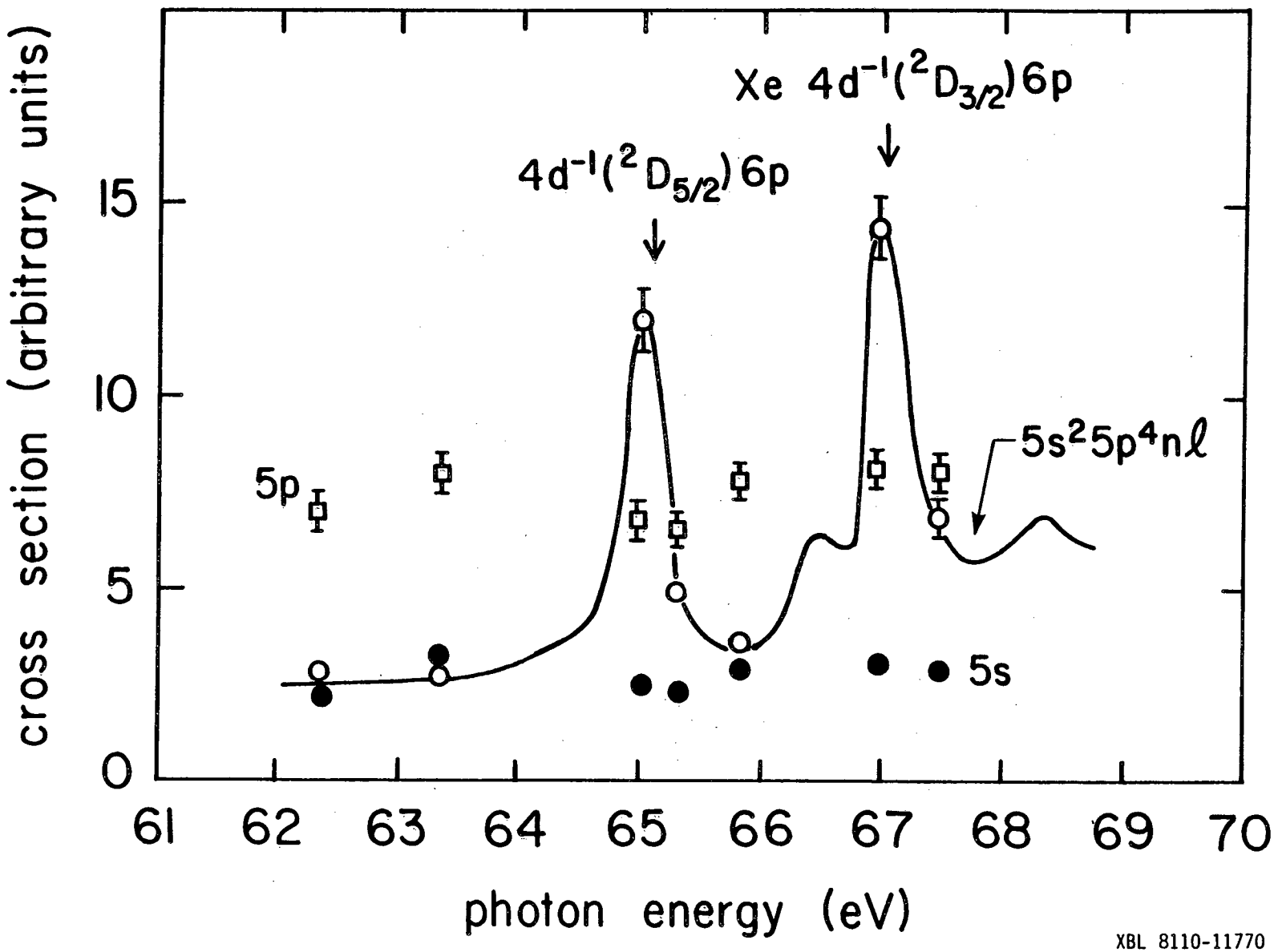

XBL 8110-11770

Figure 13

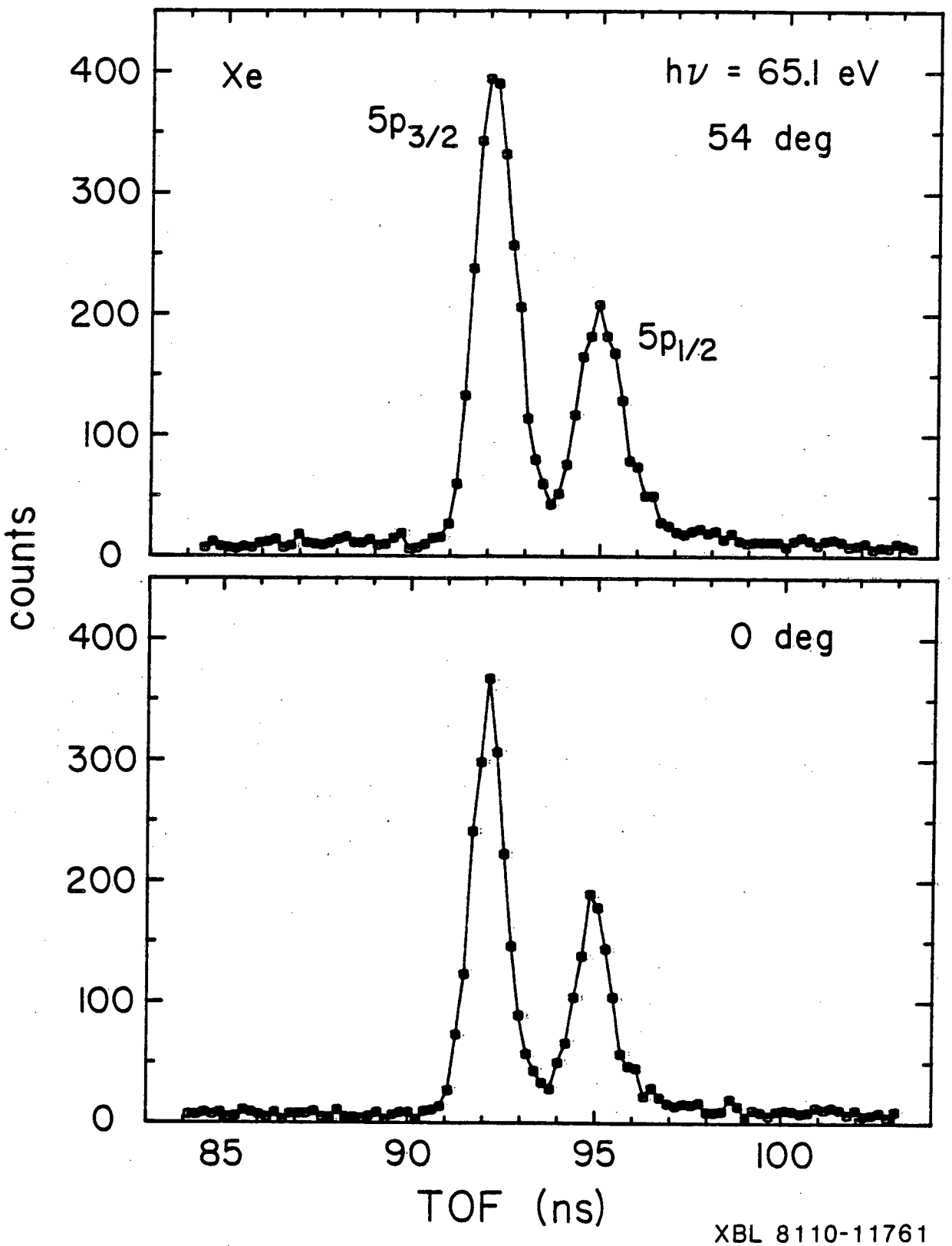
Xe
hν = 65.1 eV
54 deg
5p3/2
5p1/2
0 deg
counts
400
300
200
100
0
85
90
95
100
TOF (ns)
XBL 8110-11761

Figure 14

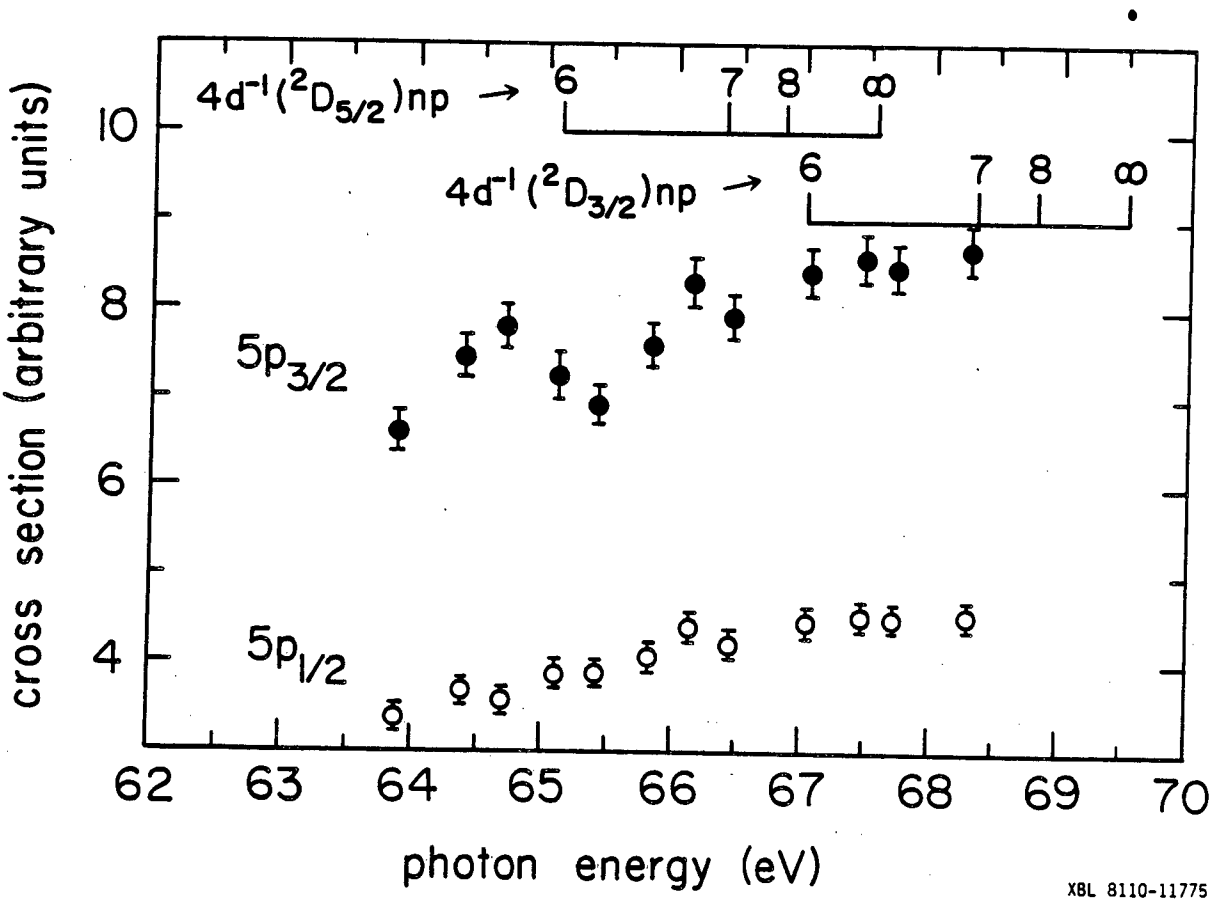
4d⁻¹(²D5/2)np →
6
7
8
∞
4d⁻¹(²D3/2)np →
6
7
8
∞
5p3/2
5p1/2
cross section (arbitrary units)
10
8
6
4
62
63
64
65
66
67
68
69
70
photon energy (eV)
XBL 8110-11775

Figure 15

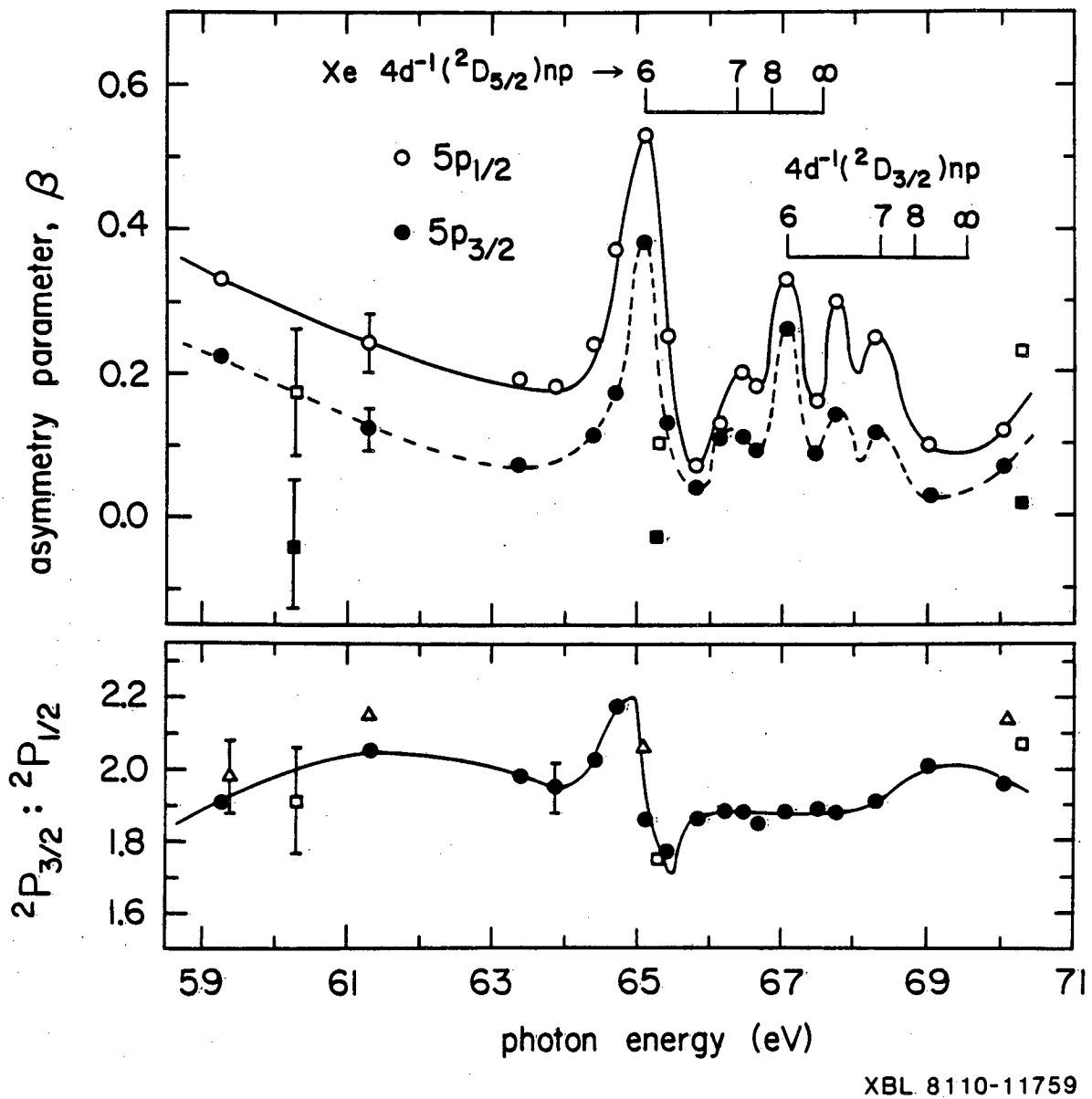
Xe 4d⁻¹(²D5/2)np → 6 7 8 ∞
5p1/2
5p3/2
4d⁻¹(²D3/2)np
6 7 8 ∞
asymmetry parameter, β
0.6
0.4
0.2
0.0
²P3/2 : ²P1/2
2.2
2.0
1.8
1.6
59
61
63
65
67
69
71
photon energy (eV)
XBL 8110-11759

Figure 16

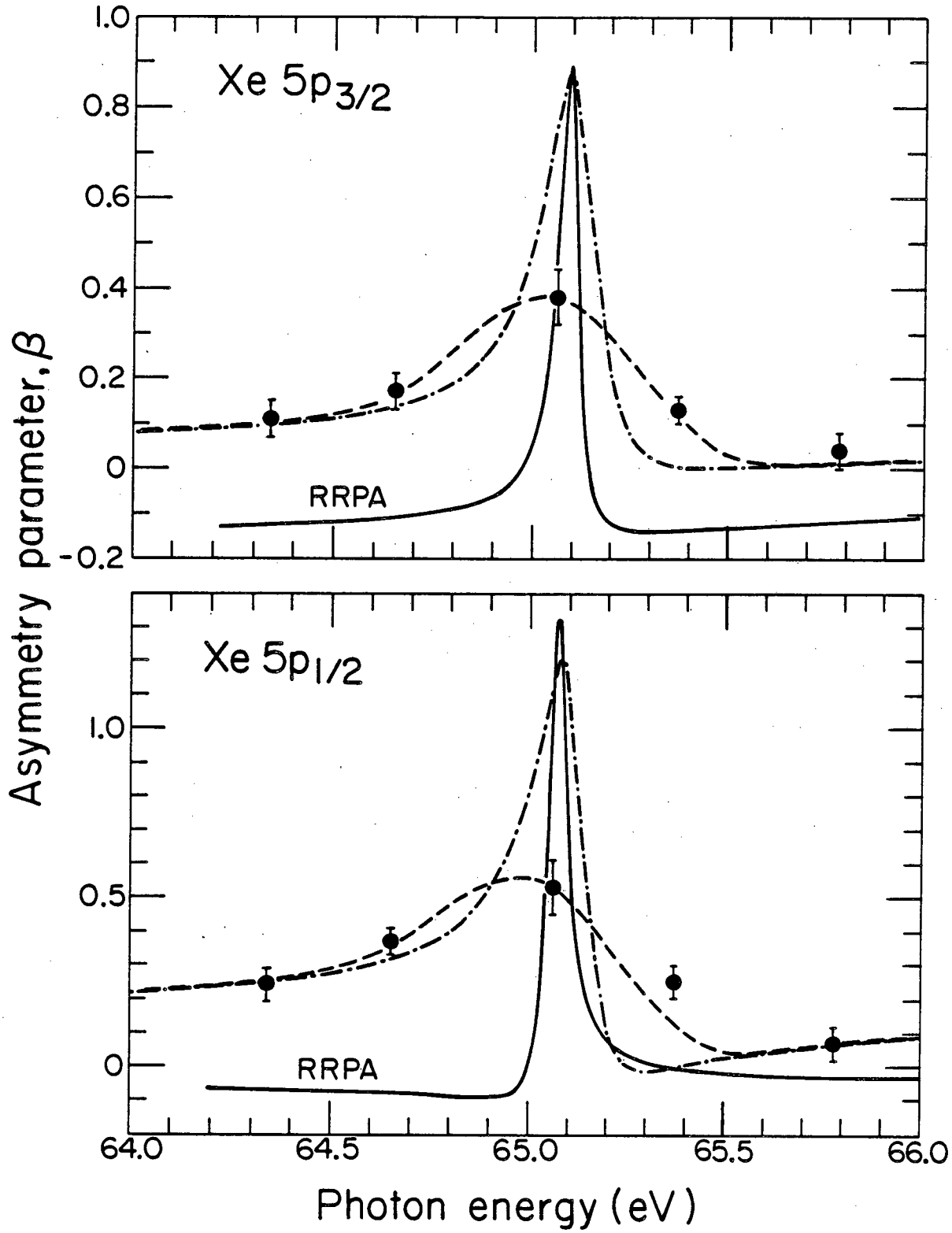

XBL8111-12064

Figure 17

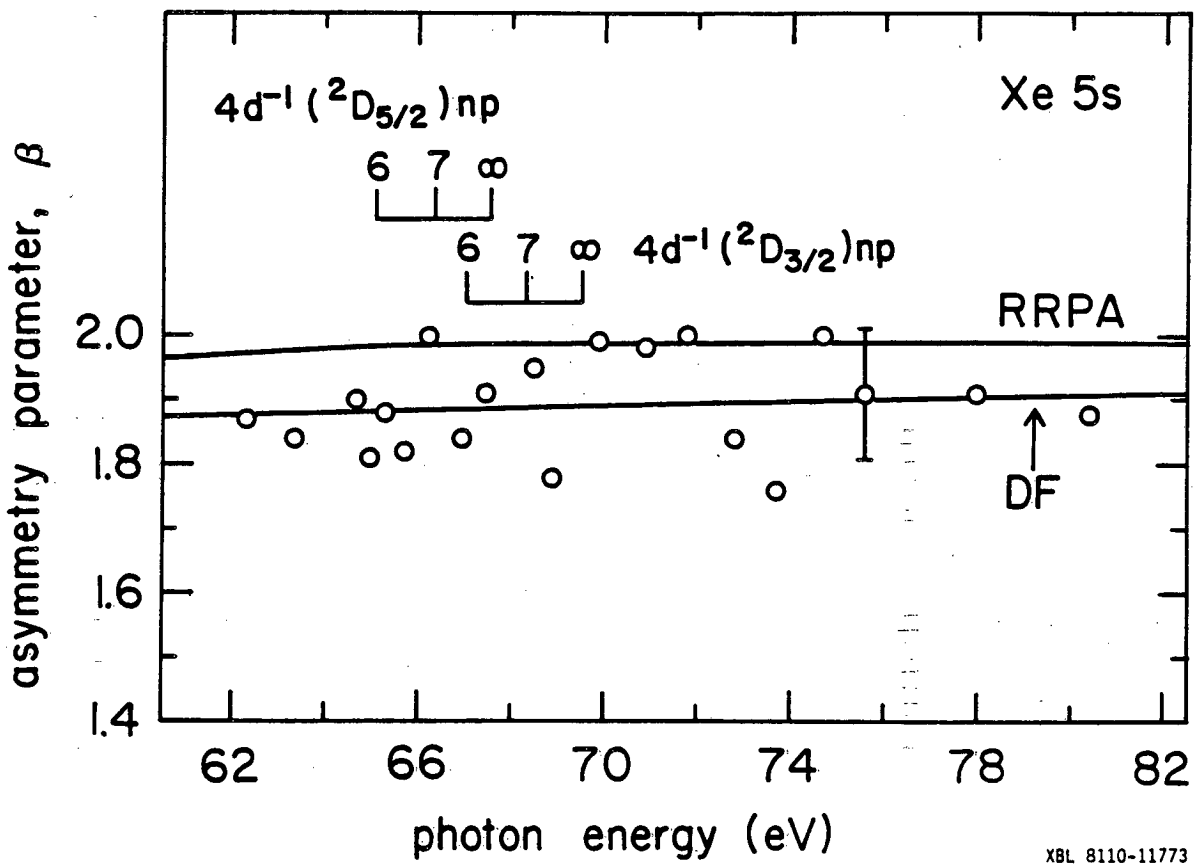
4d⁻¹(²D5/2)np
6 7 ∞
6 7 ∞ 4d⁻¹(²D3/2)np
Xe 5s
RRPA
DF
asymmetry parameter, β
2.0
1.8
1.6
1.4
62
66
70
74
78
82
photon energy (eV)
XBL 8110-11773

Figure 18

TECHNICAL INFORMATION DEPARTMENT
LAWRENCE BERKELEY LABORATORY
UNIVERSITY OF CALIFORNIA
BERKELEY, CALIFORNIA 94720

This report was done with support from the Department of Energy. Any conclusions or opinions expressed in this report represent solely those of the author(s) and not necessarily those of The Regents of the University of California, the Lawrence Berkeley Laboratory or the Department of Energy.

Reference to a company or product name does not imply approval or recommendation of the product by the University of California or the U.S. Department of Energy to the exclusion of others that may be suitable.